2014

Deformation mechanisms in mylonites at Fletcher Peak, Washington County, ME

Ariana S. Boyd
Colby College

DEFORMATION MECHANISMS IN MYLONITES AT FLETCHER PEAK, WASHINGTON COUNTY, ME

Ariana S. Boyd ‘14

A Thesis

Submitted to the Faculty of the Geology Department of Colby College in Fulfillment of the Requirements for Honors in Geology

Waterville, ME

May 2014

Abstract

Mylonite formation and development is dependent on a number of factors including temperature, strain rate, and fluid fugacity. All three factors affect flow stress and viscosity; thus, a variance in each will affect the development of mylonites. This study focuses on factors leading to the formation of mylonite surrounded by ultramylonite of the same protolith, along-strike to one another at the center of a fault zone. The rocks in question are from the Deblois granite cut by the Kellyland fault zone, a ductile strike-slip fault zone within the larger Norumbega fault system in eastern Maine. The Deblois granite as a whole experienced three stages of deformation within the Kellyland fault zone: a primary high-temperature phase, a second brief brittle phase, and a third long-lived ductile phase. The brittle phase prompted the widespread development of ultramylonite in the center of the shear zone; the zone of mylonite records no evidence for this brittle phase. The lack of brittle deformation in the mylonites was probably due to prolonged locally elevated temperatures and to a high fluid content during later stages of deformation. The implications for this study are that even in a setting of prolonged high-strain shearing, ultramylonites may not form without a primary brittle phase to weaken the overall rheology, and may not form in the presence of a fluid.

Acknowledgments

I would first like to thank Dr. Walter A. "Bill" Sullivan for all the ways he helped make this project a success: his edits, comments, insight, and help both in the field and in the laboratory. Thanks to Drs. Bob Gastaldo, Bob Nelson and Bruce Rueger for their comments, edits, and understanding throughout the year. Many thanks to Chuck Jones for his time and efforts in fixing every instrument that malfunctioned under my use. Thanks to Justin Sperry for his help in the field collecting samples. Thanks to Dr. Don Allen for helping me operate and understand Colby's SEM and XRD, and to Dr. Rachel Beane for her help and patience with my use of the EBSD at Bowdoin College. Finally, thank you to Alice Ridky for somehow making things run smoothly all year; to my friends and fellow students for their support and understanding; and to my family for their love and support.

This project was funded by the Claire Boothe Luce Foundation, by the Colby College Division of Natural Sciences, and by the Colby College Geology Department.

Table of contents

1. Introduction

Mylonitic rocks are foliated high-strain rocks formed in ductile shear zones under low- to medium-grade metamorphic conditions (Sibson, 1977; Trouw et al., 2009). Because they are relicts of past shear zones, mylonites are excellent primary sources for understanding the tectonic history of an area. These high-strain rocks record the conditions under which a fault zone was active and the movement direction(s) of the fault (Lister and Snoke, 1984; Greene and Schweickert, 1995; Snoke et al., 1998; Trouw et al., 2009). Mylonites also record the deformation mechanisms that controlled the rheology of that fault zone (Handy et al., 2007). In the field, mylonites are subdivided into three categories by their matrix-to-porphyroclast ratio (Sibson, 1977; Snoke et al., 1998; Trouw et al., 2009). Protomylonites contain up to 50% matrix by volume; mylonites contain 50-90% matrix; and ultramylonites contain upwards of 90% matrix. It traditionally has been assumed that mylonite development was the progressive result of increasing ductile deformation with no change in deformation mechanisms (e.g., Bell and Etheridge, 1973); however, all three mylonite types commonly are found in the same shear zone, and mylonites and ultramylonites often are interlayered with no other evidence for variations in strain intensity (e.g., Hippertt and Hongn, 1998; Bailey and Eyster, 2003; Wang and Ludman, 2004; Price et al., 2012; Sullivan et al., 2013). These occurrences indicate that spatial variations in deformation mechanisms, rather than variations in strain intensity, may form different mylonitic rocks.

Although mylonitic rocks are common, the mechanisms by which they form still are not understood fully. Crustal-scale ductile shear zones originate from localized shear zones catalyzed by strain softening (Platt and Behr, 2011). Strain softening is driven by one of four potential mechanisms: 1) chemical alteration and accompanying phase changes (O'Hara, 1988; Stunitz

and Fitz Gerald, 1993; Hippertt and Hongn, 1998); 2) interconnection of weak mineral phases (e.g., Tullis, 2002); 3) dynamic recrystallization and consequent grain-size reduction; or 4) cataclasis and/or melting, and resultant brittle grain-size reduction and phase mixing (e.g., Handy et al., 2007; Price et al., 2012). We do not yet completely understand which strain-softening process or processes are most important in different rock types at different crustal levels and/or metamorphic grades. Moreover, these processes often operate synchronously (e.g., Tullis and Yund, 1987; Hippertt and Hongn, 1998), which further complicates understanding their roles in strain softening. The grain-size reduction that forms the matrix of mylonitic rocks can dramatically alter rock rheology, and different deformation mechanisms can operate in rocks with different grain sizes at the same temperature and strain rate (e.g., Wintsch and Yeh, 2013). These variables are complicated and difficult to reproduce experimentally, further complicating the problem; thus, detailed studies of deformation mechanisms in naturally formed mylonites are needed. To this end, I offer a detailed analysis of mechanisms driving the formation of naturally deformed mylonitic rocks from the Kellyland fault zone (KFZ) in eastern Maine.

The KFZ is a ductile strike-slip shear zone that juxtaposes homogeneous granite of the Deblois pluton with metasedimentary rocks (Figs. 1, 2). Rocks cut by the KFZ were deformed at greenschist-facies conditions in the middle Devonian (Ludman et al., 1999, 2000; Wang and Ludman, 2004). The progressive deformation of the Deblois granite is preserved in different spatial domains of the shear zone. The center of the shear zone records the final and most long-lived phase, and it is marked by a 200-400-m wide belt of granite-derived ultramylonite (Sullivan et al., 2013). Within this ultramylonite zone is a discrete zone of mylonite (Fig. 2B). While the total extent of this mylonite zone is not exposed, it can be traced across the entire width of the ultramylonite zone in one extensive exposure at Fletcher Peak (Figs. 2B, 3). Such a

pronounced change in fault rock type along-strike in a single protolith prompts the question: why is deformed Deblois granite in this location mylonite as opposed to ultramylonite?

2. Background

2.1 Regional geology

The Kellyland fault zone lies within the larger Norumbega fault system (NFS), a long-lived, orogen-parallel, dextral strike-slip system that lies parallel with the coastline of Maine (Hubbard, 1999; Ludman and West, 1999). The NFS formed during the earliest stages of the Neo-Acadian orogeny around 380 Ma (Ludman and West, 1999; Ludman et al., 2000) as a result of oblique transform activity between North America and the accreting terranes (Gerbi and West, 2007). In eastern Maine, the NFS consists of three fault zones: the northernmost Codyville fault zone (CFZ), the Waite fault zone (WFZ), and the southernmost Kellyland fault zone (KFZ) (Ludman and West, 1999; Wang and Ludman, 2004). All three range from 0.5 to 5 km wide and record mid-Devonian greenschist-facies ductile deformation (Ludman et al., 1999; Wang and Ludman, 2004). The Codyville and Waite fault zones also record significant late-stage brittle overprinting; however, the KFZ records little brittle overprinting (Ludman et al., 1999; Wang and Ludman, 2004). The KFZ juxtaposes homogeneous granite of the Deblois pluton and metasedimentary rocks of the Flume Ridge Formation (FRF); this study focuses on the granitic rocks cut by the KFZ.

2.2 Deblois granite cut by the KFZ

The Deblois granite is the largest singular pluton in a suite of Devonian intrusive rocks in this portion coastal Maine (Fig. 1) (Osberg et al., 1985; Wang and Ludman, 2004; Sullivan et al.,

2013). Undeformed Deblois granite is texturally uniform and homogeneous (Fig. 4) (Riley, 2004). It contains microcline, plagioclase (in tabular grains and as Rapakivi-type rims on microcline), biotite, quartz, and hornblende as major phases. Trace phases include zircon, ilmenite, titanite, apatite, and allanite (Wang and Ludman, 2004; Sullivan et al., 2013). Deblois granite cut by the KFZ exhibits three distinct strain-facies-defined domains from the margins of the shear zone to the center of the zone (Fig. 2) (Sullivan et al., 2013). These are the foliated granite domain, the localized shear zone domain, and the main ultramylonite domain.

The foliated granite domain extends 2-3 km across strike (Fig. 2) and consists of variably foliated Deblois granite with local undeformed zones. In these rocks, elongated quartz and biotite grains define the weak foliation. Feldspars in foliated granite are largely undeformed aside from some local flattening and rotation to alignment with quartz and biotite grains (Sullivan et al., 2013). The localized shear zone domain extends 100-300 m across-strike and consists of localized bands of mylonite and ultramylonite cutting foliated Deblois granite. Localized shear zones have both abrupt and gradational boundaries with the foliated granite (Sullivan et al., 2013). These shear zones nucleated on recrystallized cataclasite and pseudotachylite veins, although no fabrics suggestive of cyclical brittle-and-ductile overprinting are visible (Sullivan et al., 2013). The main ultramylonite domain extends 200-400 m across-strike (Fig. 2A). Ultramylonite in the ultramylonite domain ranges from homogeneous to pinstripe ultramylonite. Homogeneous ultramylonites are macroscopically uniformly gray and flinty; microscopically, they contain a uniform matrix that is an ultra-fine-grained mixture of two feldspars + biotite +/- quartz. In pinstripe ultramylonites, recrystallized feldspar and quartz are discretely interlayered in 0.5-5-mm-wide bands (Sullivan et al., 2013). There is also a large area of mylonite centered about Fletcher Peak and adjacent to a quartz diorite body also cut by the KFZ (Figs. 2, 3). The

along-strike length of the mylonite band cannot be accurately constrained, but one excellent continuous exposure reveals that it extends across the entire width of the main ultramylonite domain at Fletcher Peak. These three domains preserve fabrics from different temporal stages of deformation in the KFZ.

The foliated granite records the earliest stage of deformation, a short-lived high-temperature phase. Dislocation creep of quartz and, to a lesser extent, solution transfer of feldspar, governed the rheology during this first phase of deformation (Sullivan et al., 2013). The localized shear zones originated from brittle fractures and represent a discrete brittle phase of deformation. The main ultramylonite zone represents the final stage of deformation; a long-lived period of ductile deformation that overprinted all other fabrics (Sullivan et al., 2013). Extensive phase mixing in ultra-fine-grained aggregates in homogeneous ultramylonites indicates deformation by granular flow. Pinstripe ultramylonites exhibit extensive subgrain-rotation recrystallization of quartz, indicating deformation by dislocation creep of quartz. Microstructures in pinstripe ultramylonite indicating dynamic recrystallization of feldspars and, hence, deformation by dislocation creep are interpreted as relict structures from earlier higher-temperature deformation (Sullivan et al., 2013). Frequent sharp grain boundaries in feldspar aggregates in pinstripe ultramylonites also indicate deformation by the granular flow mechanism (Sullivan et al., 2013).

3. Methods

I went into the field in the summers of 2012 and 2013 and made observations of granitic mylonite and ultramylonite cut by the KFZ. I recorded the extent and intensity of deformational fabrics, presence or absence of quartz veins and dikes, and, where veins and dikes were present,

the extent to which they are deformed. I took measurements of foliation and lineation orientation, and the orientations of quartz veins and leucogranite dikes. I also collected samples, with the help of M.E. Monz, J.A. Sperry, and W.A. Sullivan, using a core drill, and a hammer and chisel. Samples were collected in the summers of 2011, 2012, and 2013 from mylonitic granite, diorite, quartz veins and leucogranite dikes at the Fletcher Peak locality (Table 1). Because most outcrops are weathered throughout, fresh samples of foliated rocks were prioritized over oriented samples. Samples collected by W.A. Sullivan in 2011 are of granite-derived mylonite, ultramylonite and leucogranite dikes. Samples collected by W.A. Sullivan, M.E. Monz, and A.S. Boyd in 2012 are of granite-derived ultramylonite, foliated granite, and undeformed granite. Samples collected by W.A. Sullivan, J.A. Sperry and A.S. Boyd in 2013 are of granite-derived mylonite, foliated and undeformed diorite, quartz veins within foliated diorite, and leucogranite dikes.

In the lab, I analyzed mineralogy, quartz recrystallized grain size, and crystallographic preferred orientations (CPOs). I also made detailed microstructural observations. Thin sections were made from cuts perpendicular to foliation and parallel with lineation for transmitted-light and scanning-electron microscopy (SEM). Samples that did not exhibit chemical weathering or late-stage metasomatism were crushed, powdered, and homogenized for x-ray diffractometry (XRD) analyses and bulk-rock geochemical analyses. Powdered homogenized samples were sent to Actlabs, Ontario, Canada for ICP, INAA and XRF analyses to determine bulk-rock geochemistry.

Bulk-rock geochemical data from Actlabs was used to create isocon plots of granitic mylonites and ultramylonites relative to undeformed and foliated granite, in order to determine any changes in relative chemical abundance. These plots show elemental variations in mylonites

& ultramylonites versus undeformed granite and are useful for determining if loss or gain of major or trace elements occurred (e.g., O'Hara, 1988).

I used a variety of techniques to determine bulk mineralogy and the mineralogy of individual domains within samples. Bulk mineralogy was determined using a Rigaku Geiger-flex powder X-ray diffractometer, MDA DataScan 3.2 software and MDI Jade 9 analysis software. I pressed powdered samples onto 0.5-mm depressions in glass slides. I used DataScan to run the samples in a continuous scan with an initial theta value of 1.5. After collecting peak patterns with DataScan, I opened each peak pattern in Jade 9, corrected the background height, and used an RBD-IBSD minerals package to match each peak with the correct mineral phase based on closest matches. This system produced accurate results for all major mineral phases except for triclinic feldspars. Because the triclinic feldspars in these rocks are products of prolonged solid-state exsolution, their crystal lattices are hard to distinguish with X-ray diffractometry.

To understand the dominant deformation mechanisms that operated in each sample, I conducted microstructural analyses using a standard transmitted-light petrographic microscope. Evidence for deformation by dislocation creep includes quartz and feldspar recrystallization via grain boundary bulging, subgrain rotation, and grain-boundary migration (Hirth and Tullis, 1992; Stipp et al., 2002). Evidence for deformation by solution-precipitation creep includes pressure-shadow wings on porphyroclasts, dilatational fractures, and pressure-solution seams along the edges of porphyroclasts (Wintsch and Yi, 2002; Passchier and Trouw, 2005). Microstructures indicative of deformation by the granular flow mechanism are 1) extremely small, uniform grain size; 2) equant recrystallized grains; and 3) homogeneous polyphase aggregates, and grain shapes indicative of grain-boundary sliding (Stunitz and Fitz Gerald, 1993; Sullivan et al., 2013).

To investigate any preferential alignment of recrystallized quartz grains, I measured crystallographic orientations using the SEM at Bowdoin College, ME, which is equipped with an HKL Nordlys II detector and complemented by Channel 5 software, following the method of Beck (2012). I used a 40-μm step size for collecting quartz crystallographic data because, unlike Beck, I am primarily interested in the bulk CPO in recrystallized quartz domains. A moderate to strong CPO in recrystallized quartz is indicative of deformation by dislocation creep; a lack of CPO can indicate deformation by either dissolution-precipitation creep or by the granular flow mechanism (Menegon et al., 2008). Quartz c-axis fabrics also can record deformation-temperature variations between samples (Passchier and Trouw, 2005, and references therein).

Quartz recrystallized grain size is dependent on differential stress during deformation (Hirth and Tullis, 2002; Stipp et al., 2002). Hence, variations in quartz recrystallized grain size may record variations in deformation conditions throughout the shear zone. To measure recrystallized quartz grain size, I collected micrographs using a Nikon DS-Ri1 camera mounted on a Nikon Eclipse LV100 POL transmitted-light microscope, and measured the long and short axes of 200 recrystallized quartz grains per sample using a measuring tool in the software program NIS-Elements BR v. 3.1. These analyses were conducted on at least two quartz-rich domains from each thin section.

4. Field relationships

4.1 Granite-derived mylonite

The contact between the mylonite domain and the surrounding ultramylonite is hidden, but the mylonite domain spans at least 500 meters along-strike and spans the entire width of the main ultramylonite zone (Figs. 2B, 3). Foliations in mylonite strike northeast and dip steeply to

the southeast (Fig. 5). Mylonites at Fletcher peak are pinstripe-colored in hand sample and contain abundant 2-30-mm-wide feldspar porphyroclasts and 1-5-mm-wide quartz ribbons and biotite-rich bands (Fig. 6). Many of these biotite-rich bands and feldspar porphyroclasts are oblique to the main foliation. Mylonite at Fletcher Peak also hosts numerous quartz veins and leucogranite dikes. All of the veins and dikes I observed are foliated and nearly parallel with the foliation in adjacent granitic mylonites (Figs. 5, 7).

4.2 Quartz diorite

At Fletcher Peak, the quartz diorite is visible for 40 m across-strike. All quartz diorite is foliated, and some foliated quartz diorite is brecciated at the contact between the quartz diorite and the Deblois granite. The deformed quartz diorite contains hornblende, plagioclase feldspar, quartz, tremolite, and minor biotite and microcline. The quartz-diorite body is macroscopically heterogeneous and contains alternating 1-9-mm-wide amphibole-rich and feldspar-rich bands. The mafic layers are green-black in color and the felsic areas are gray in color. Foliations across the quartz diorite are uniformly oriented, and the grain size is uniform throughout.

4.3 Quartz veins and leucogranite dikes

Quartz veins at Fletcher Peak occur throughout the granitic mylonite and diorite. They range from 1 to 15 cm in width. All quartz veins are foliated and are aligned subparallel with regional foliation. Out of 11 quartz veins observed at Fletcher Peak, 6 are directly in contact with leucogranite dikes. Intersecting dikes and veins are subparallel (Fig. 7C).

Leucogranite dikes range in width from about 5 cm to >2 m across strike and occur throughout the Deblois granite mylonite and diorite. The dikes are variably deformed. Some

dikes contain feldspar porphyroclasts up to 3 mm in length whereas others are entirely fine grained. Fine-grained deformed dikes are interpreted to have fine-grained, aplitic protoliths whereas deformed dikes with prominent porphyroclasts probably had coarse-grained to pegmatitic protoliths. The dikes all contain plagioclase, potassium feldspar, quartz, and muscovite. Intensity of deformation between adjacent dikes, veins, and Deblois granite mylonite appears similar; all granitic rocks are more than 50% recrystallized with a fine-grained and foliated matrix, and quartz veins are completely recrystallized and uniformly foliated.

5. Geochemistry of granite samples

Major- and trace-element concentrations were measured in two samples of undeformed granite, three samples of foliated granite (Sullivan et al., 2013), and three samples of granite mylonite. Results of analyses are listed in Tables 2 and 3. Geochemistry data from the undeformed and foliated granite samples were combined to produce an average granite bulk geochemical composition, and isocon graphs plotting each granite mylonite sample against this average granite composition were made (Fig. 8). To determine the amount of volume loss recorded by each granite mylonite sample, bulk change in volume was calculated for each isocon plot. Bulk-rock change in volume (Δ) is defined as:

$$C_f/C_i = 1/(1+ \Delta).$$

where C_f is the final concentration of a rock (in this case, each granite mylonite composition) and C_i is the initial concentration (the average granite composition) (O'Hara, 1988). The ratio C_f/C_i is the slope of each equation, and is calculated from a best-fit linear trendline applied to each graph. All slopes and Δ values are written on each graph in Figure 8.

Best-fit linear trendlines for all three graphs have slopes slightly above 1, indicating a slight overall volume loss from undeformed granite to mylonite (O'Hara, 1988; Bailey et al., 1993).

6. Microstructures

6.1 Deblois granite mylonite

Granitic mylonites derived from the Deblois pluton contain microcline, plagioclase, quartz, biotite, hornblende, and minor apatite and zircon (major phases listed in Table 4). Almost 100% of microcline, plagioclase, biotite, and hornblende grains show evidence for crystal-plastic deformation. Primary microcline grains are largely perthitic, and a number of recrystallized microcline porphyroclasts also exhibit flame perthite (Figs. 9A-B ,9F). Both microcline and plagioclase feldspar porphyroclasts appear to break preferentially along twin planes, when twins are present in grains. Microcline porphyroclasts display sweeping to patchy undulose extinction (Figs. 9A, 9B). Recrystallized feldspar grains are 6-80 μm in diameter, and are generally oriented subparallel with foliation. Microcline also occurs as elongated, partially recrystallized ribbons of disaggregated porphyroclasts and neoblasts (Fig. 9D). Quartz- and k-feldspar-filled dilatational fractures and quartz pressure-shadow wings are common in partially recrystallized microcline grains (Figs. 9F, 9G); similarly, potassium feldspar- and quartz-filled dilatational fractures are common in plagioclase. Plagioclase feldspar porphyroclasts, in contrast to microcline, are often untwinned and often exhibit bookshelf fractures and pull-apart structures of blocks of plagioclase parallel to cleavage planes (Fig. 9D). Plagioclase grains typically exhibit sweeping extinction in larger grains or patchy extinction in more recrystallized areas. Some plagioclase grains contain myrmekitic intergrowths of quartz and potassium feldspar in high-strain sites (Fig. 9E). Both microcline and plagioclase are often partially or completely rimmed

by neoblasts. Quartz pressure shadow wings also occur on plagioclase grains (Fig. 9F), but these are less common on plagioclase than on microcline. Many feldspars are bounded by solution seams of micaceous and opaque material on foliation-parallel faces (Figs. 9, 10).

Quartz in granitic mylonites appears in two principle domains: first, in masses of recrystallized primary grains, either as ribbons or as lenticular aggregates, and second, overgrowing feldspar in porphyroclast wings or replacing feldspar in quarter-structure sites. Recrystallized quartz grain sizes range from 5 μm to 100 μm in diameter with an average size of 20 μm (Table 5; Fig. 10A). Granite mylonites contain two classes of recrystallized quartz grains: small, relatively equant neoblasts that are 2-10 μm in diameter, and larger, amoeboid grains that are 6-60 μm in diameter (Figs. 10A, 10B). Larger amoeboid recrystallized quartz grains contain smaller subgrains that are roughly the size of the smaller neoblasts. All of these features indicate relief of internal strain energy via dislocation creep (e.g., Hirth and Tullis, 1992; Stipp et al., 2002). The larger, amoeboid grains are indicative of strain recovery via grain boundary migration recrystallization; the smaller equant recrystallized quartz grains, and subgrains of the same size within larger amoeboid quartz grains, are a typical feature of recovery via subgrain rotation recrystallization (Hirth and Tullis, 1992; Stipp et al., 2002).

Hornblende in mylonites derived from Deblois granite often is completely or partially altered to biotite and/or actinolite. Most relict hornblende grains exhibit sigma-type porphyroclast wings and biotite +/- actinolite replacement on their margins (Figs. 11A-C). Biotite in these rocks is either partially recrystallized or completely recrystallized. Relict biotite grains are preferentially oriented subparallel with the foliation and are fish-shaped to irregular. Biotite also occurs in the abundant pressure-solution seams on foliation-parallel faces of partially recrystallized feldspars (Figs. 9E and 9F).

Zircon and apatite occur as minor phases in granitic mylonite. Apatite always occurs as inclusions in hornblende porphyroclasts, and zircon occurs randomly throughout all samples. Epidote, clinozoisite, and titanite occur as trace phases. Ilmenite occurs as opaque masses in biotite-rich areas throughout the mylonite.

6.2 Quartz diorite

The quartz diorite contains plagioclase feldspar, hornblende, quartz, tremolite, biotite, and minor microcline (major phases listed in Table 4). Quartz comprises 15-20% of the quartz diorite. Tremolite occurs primarily as a pseudomorph of hornblende; tremolite pseudomorphs, hornblende porphyroclasts, and feldspar porphyroclasts are 20% to 100% recrystallized.

Plagioclase feldspar in quartz diorite is found as partially recrystallized porphyroclasts and subordinate neoblasts surrounding relict grains. Plagioclase porphyroclasts exhibit abundant dilatational fractures (Figs. 12A, 12C) and pressure shadow wings (Figs. 12A, 12C). All porphyroclasts are oriented subparallel with the compositional layering and are interwoven with other mineral phases (Fig. 12B). Quartz has precipitated in almost all dilatant sites (Figs. 12A, 12B). Of the few microcline grains present in the quartz diorite, almost all contain quartz-filled pressure-shadow wings and/or dilatational fractures (Fig. 12C). Many feldspars are rimmed by pressure-solution seams of biotite and minor opaque phases (Fig. 12C). Quartz grains in the quartz diorite occur as rare ribbons, as elongate aggregates of recrystallized grains, as replacement minerals in feldspar wings, and as precipitates in dilatational sites in and around feldspar porphyroclasts (Figs. 12A-C). Recrystallized quartz grains in the diorite range from 9-83 μm in diameter, and have an average size of 36 μm (Table 5). Recrystallized quartz grains in the quartz diorite also appear in two distinct classes: first, as larger, elongate and amoeboid

recrystallized grains, and second, as smaller, equant subgrains and neoblasts often rimming larger irregularly shaped grains. Hornblende is abundant in the quartz diorite primarily as rotated porphyroclasts surrounded by fine-grained masses of biotite, tremolite, and opaque phases. The opaque phase in these fine-grained aggregates is most likely siderite.

6.3 Leucogranite dikes

Leucogranite dikes range from mylonitic coarse-grained to pegmatitic leucogranite to intensely deformed aplite. All leucogranite dikes contain quartz, microcline, plagioclase, and muscovite. Foliation in both coarse-grained and aplitic dikes is defined by bands of recrystallized muscovite. Muscovite also forms discrete bands and ~40 μm-wide lenticular aggregates rimming feldspar porphyroclasts and quartz ribbons. Feldspars in all leucogranite dikes occur mainly as partially recrystallized porphyroclasts up to 1.5 mm in width. Almost all feldspars exhibit at least partial replacement by quartz. Many feldspars exhibit quartz pressure-shadow wings and quartz replacement at quarter-structure sites (Figs. 15A-B). Myrmekite is present in some plagioclase grains (Fig. 15C). It forms throughout some grains and preferentially at high-strain sites in others. Quartz in leucogranite dikes occurs mainly as recrystallized grains interspersed with feldspars, rather than as compositionally distinct layers (Fig. 16). Quartz also occurs as a replacement mineral in feldspar pressure shadow wings and high-strain sites, and as a precipitate in dilatant sites in feldspars. White mica occurs as bands of recrystallized material, partially altered feldspars (Fig. 14), and as pristine mica fish (Fig. 17). These fish are all lenticular in shape; many have been partially separated by microfaults. Some have been split along basal planes (Fig. 17B) or fold hinges (Fig. 17C). Based on a) the microfaults and splitting along fold

hinges in mica fish, and b) that all definitively metamorphic mica is fine-grained and concentrated in bands, the mica fish are probably porphyroclasts.

6.4 Quartz veins

Quartz veins occur throughout all lithologies at Fletcher Peak. All are foliated, lineated, and oriented subparallel with the regional foliation. All grains in quartz veins are free of dislocations and are strain-free, indicating that quartz grains in the quartz veins are 100% recrystallized. Recrystallized quartz grains are elongate and contain roughly equant subgrains (Fig. 18). There are no larger amoeboid recrystallized grains in the quartz veins.

6.5 Lattice preferred orientations (LPOs)

Crystallographic preferred orientations (CPO), also called lattice-preferred orientations (LPO), within a fabric are often visualized as density plots on stereograms, called fabric skeletons, where *c*- and *a*-axis fabric densities are plotted by their obliquity to the reference plane, which is plotted horizontally.

Crystallographic orientations of quartz grains were measured in a quartz ribbon derived from a primary igneous grain in granite mylonite (sample FP03-A), and in a quartz vein hosted within the quartz diorite (sample FP07-A) (Fig. 19). Data from both sections are presented in Figure 19. The quartz ribbon in the granite mylonite yielded a c-axis fabric with maxima centered about the y-axis and two smaller maxima ~30º to the y-axis, and an a-axis fabric with maxima distributed around the x-axis at the edge of the stereonet (Fig. 19B). This fabric pattern is suggestive of activity on both rhomb <a> and prism <a> slip systems (Schmid and Casey, 1986). The quartz vein in the quartz diorite yields a c-axis fabric that defines a single girdle

oblique to the foliation and a maxima near the center of the plot (Fig. 19A). A-axis maxima from this sample lie near the margins of the plot and are asymmetrically distributed about the presumed subhorizontal lineation. This fabric pattern is indicative of prism <a> slip as the dominant slip system (Schmid and Casey, 1986).

7. Discussion

7.1 Significance of the granite mylonite

Four lines of evidence aid in determining deformation conditions of granite mylonite at Fletcher Peak: 1) the quartz microstructures, 2) the quartz crystallographic fabric data from quartz in sample FP03, 3) the microcline and plagioclase feldspar microstructures and textural relationships with other phases, and 4) the bulk chemical compositions of granite mylonites across the exposure. The quartz microstructure is characterized by amoeboid quartz grains in which smaller, equant subgrains are sometimes visible, along with neoblasts that are the same size as the subgrains. The amoeboid recrystallized grains indicate that quartz initially underwent recrystallization via grain-boundary-migration recrystallization (e.g., Hirth and Tullis, 1992; Stipp et al., 2002). The overprinting of smaller subgrains indicates that deformation conditions changed such that quartz underwent subgrain-rotation recrystallization, following a period of deformation during which quartz recovered via grain-boundary-migration recrystallization. CPO data from the quartz ribbon in sample FP03-A and the quartz vein in sample FP07-A also record deformation at higher temperatures; both CPO fabric patterns indicate that prism <a> and rhomb <a> are the acting slip systems; these normally operate at temperatures between 450º-650ºC (Stipp et al., 2002; Peternell et al., 2010).

The evidence for multiple deformation mechanisms operating in quartz is compounded by evidence from feldspar microstructures. Microcline grains in granite mylonites at Fletcher Peak also contain evidence for multiple deformation mechanisms. Firstly, numerous microcline porphyroclasts exhibit flame perthite, a texture generally indicative of deformation by dislocation glide (e.g., Passchier, 1982). Both microcline and plagioclase porphyroclasts also commonly exhibit undulose and/or patchy extinction due to intragranular dislocations; this too is indicative of deformation by dislocation creep (e.g., Tullis and Yund, 1987; Hirth and Tullis, 1992; Stipp et al., 2002; Platt and Behr, 2011). A second set of evidence indicating deformation under a different regime includes quartz pressure-shadow overgrowths, dilatational fractures and pressure-solution seams surrounding feldspar. These microstructures are clues that dissolution-precipitation creep has occurred (e.g., Wintsch and Yi, 2002; Menegon et al., 2008). These fluid-assisted microstructures overprint the features indicative of dislocation glide (i.e. flame perthite, undulose extinction). These overprinting textures suggest that feldspars were deformed first by dislocation creep and glide (e.g., Tullis and Yund, 1985; Hirth and Tullis, 1992), and later subjected to solution transfer via dissolution-precipitation creep (e.g., Wintsch and Yi, 2002; Menegon et al., 2008).

At least two non-microstructural lines of evidence also point to the presence of water during at least the later phases of deformation. These are: 1) the abundant quartz veins; and 2) the apparent volume loss from granite mylonites at Fletcher Peak. Both of these are direct evidence that a significant amount of fluid was present during deformation, and that this fluid was transporting material through the shear zone (O'Hara, 1988; Bailey et al., 1993; Wintsch and Yi, 2002; Menegon et al., 2008). Quartz veins are the result of mobilized silica precipitating into

preexisting fractures or weak zones in a rock, and are thus direct evidence for syndeformational fluid fugacity. The volume loss in mylonites is especially important because it indicates that solution transfer must have occurred throughout all of the mylonite. Volume losses in samples FP01 and FP02-E are 12.4% and 19.2% respectively, while volume loss in FP03 is 7.6%. FP01 and FP02-E are closer to the quartz diorite than FP03, which means that at least some elemental mobility could be associated with intrusion of the quartz diorite, although this dataset is inconclusive.

7.2 Significance of the quartz diorite

The most important microstructural features for interpreting deformation conditions and timing in the quartz diorite are: 1) the quartz microstructures and 2) textures of feldspar porphyroclasts. Quartz grains in the quartz diorite, like quartz in the granite mylonites, appear as amoeboid grains in which subgrains can often be seen. Recrystallized quartz grains the same size as the subgrains sometimes rim amoeboid quartz grains. As in the granite, the amoeboid quartz grains recrystallized under grain-boundary-migration recrystallization. The subgrains and smaller grains show that a later, lower-temperature or higher-strain-rate deformation in the subgrain-rotation-recrystallization temperature range (e.g., Stipp et al., 2002) overprinted fabrics from the earlier, higher-temperature phase. This alone indicates that, at least for some period of time, the quartz diorite was subjected to elevated temperatures similar to those recorded by the granitic mylonites. Microstructures in feldspar porphyroclasts also exhibit evidence for multiple phases of deformation. Both plagioclase and subordinate microcline grains also exhibit sweeping undulose extinction and flame perthite, both of which are indicative of dislocation creep that can occur, in feldspars, at upper-greenschist facies conditions and above. Undulose extinction and

flame perthite are overprinted by dilatational fracturing and quartz pressure-shadow overgrowths. Both of these features are telling of dissolution-precipitation creep. During solution-transfer, material precipitates out of high-strain sites and into lower-strain sites, normally creating quartz pressure-shadow wings (see quartz in Fig. 20).

Together with the quartz veins, this microstructural evidence indicates that an earlier, higher-temperature phase of deformation during which feldspars deformed plastically was followed by a deformational phase in which fluid was present and enabled significant solution transfer and precipitation (e.g., Wintsch and Yi, 2002; Wintsch and Yeh, 2013).

7.3 Significance of the leucogranite dikes and quartz veins

The leucogranite dikes do not appear to record two phases of deformation, evidenced by 1) quartz microstructure indicating recrystallization under one regime, and 2) the lack of overprinting of microstructures in feldspar. First, all recrystallized quartz grains in dikes indicate strain recovery via subgrain-rotation recrystallization. The amoeboid quartz grains observed in granite mylonites and in the quartz diorite are absent in the dikes; where quartz aggregates are present, only equant grains, indicative of subgrain-rotation recrystallization (e.g., Hirth and Tullis, 1992) are visible. Secondly, feldspars do not exhibit perthitic features or undulose extinction. Rather, dilatational fractures, quartz pressure-shadow overgrowths and micaceous solution seams dominate feldspar microstructures. These features all indicate that a significant amount of solution transfer occurred in these rocks (i.e. Wintsch and Yi, 2002; Menegon et al., 2008). Moreover, the alteration of feldspar to white mica is an indicator of high fluid mobility and solution transfer processes in the dikes. The extensive phase mixing of quartz and feldspar preserved in these dikes is indicative of syndeformational nucleation of compositionally distinct

feldspar grains that preferentially occurred at dilatational sites in porphyroclasts and between grains in the matrix (e.g., Menegon et al., 2013). This solution transfer-induced phase mixing is also typical of feldspars deformed via dissolution and replacement creep (e.g., Killian et al., 2011).

Quartz veins appear to contain evidence for deformation at the upper bounds of the subgrain-rotation recrystallization regime, evidenced by 1) the quartz microstructure, and 2) the CPO pattern of a quartz vein hosted by the quartz diorite. All grains in the quartz veins are equant and appear to be strain-free; this indicates that they underwent dislocation creep and subgrain-rotation recrystallization (e.g., Hirth and Tullis, 1992; Stipp et al., 2002). The CPO pattern produced from a quartz vein hosted by the quartz diorite, however, is indicative of prism <a> slip (Stipp et al., 2002; Peternell et al., 2010). Prism <a> slip, which is recorded in the CPO fabric of the quartz vein, is generally assumed to be indicative of deformation under upper-most-greenschist- to lower-amphibolite-facies temperature conditions (Stipp et al., 2002), although dominant prism <a> slip has been found in quartz deformed at middle- to upper-greenschist-facies temperatures as well (Peternell et al., 2010). CPO data and microstructure data, then, indicate that quartz veins were subjected to a phase of mid- to upper-greenschist facies deformation where prism <a> was the active slip system, and quartz underwent subgrain-rotation recrystallization during dislocation creep (e.g., Hirth and Tullis, 1992). These lines of evidence indicate that the quartz veins were deformed under one continuous phase.

The absence of an early, high-temperature phase in the leucogranite dike, coupled with the lack of evidence for grain-boundary-migration recrystallization in the quartz veins, means that the dikes and veins were not subjected to high-temperature deformation from which fabrics are preserved in the granite mylonites and quartz diorite. Moreover, the lack of evidence for any

brittle deformation in these rocks indicates that the dikes and veins were not subjected to a phase of brittle deformation. Two constraints now can be placed on the timing and conditions of leucogranite dike intrusion and quartz vein formation and how they subsequently were deformed: 1) the dikes and veins probably formed after the initial phase of high-temperature deformation recorded in the granite mylonite domain, and 2) if dikes and veins formed during the second (brittle) phase of deformation recorded elsewhere in granite in the KFZ (e.g., Sullivan et al., 2013), then they were also not subjected to brittle deformation. This is certainly due, in part, to the extensive amount of fluid that was present, and may also be due to elevated temperatures related to syndeformational intrusion of the quartz diorite.

7.4 Evolving deformation mechanisms throughout the KFZ

Evidence from the granite mylonites, the quartz diorite, and the leucogranite dikes and associated quartz veins indicate that multiple phases of deformation, during which different lithologies were present, deformed these rocks. A study done by Sullivan et al. (2013) found that the KFZ underwent three pulses of deformation: an initial high-temperature phase, a second, brief brittle phase, and a final long-lived ductile phase.

Based on this study and on conclusions drawn by Sullivan et al. (2013), both the Deblois granite and the quartz diorite cut by the KFZ were subjected to an initial phase of high temperature (≥550º C) deformation (Wang and Ludman, 2004; Sullivan et al., 2013). During this phase, quartz deformed via dislocation creep under the grain-boundary-migration regime (e.g., Hirth and Tullis, 1992). Feldspar underwent dislocation glide +/- minor solution-precipitation creep during this phase. Quartz was probably the weakest phase across the Deblois granite, the quartz diorite, and the leucogranite dikes, although for Fletcher Peak mylonites this is not fully

established due to extreme overprinting of previous phases. The quartz diorite probably appeared during or directly after this initial phase of deformation. This conclusion can be drawn for two reasons: 1) plastically deformed feldspars in the quartz diorite contain evidence for a higher-temperature phase of deformation; 2) the diorite is cut by leucogranite dikes and quartz veins, so it must predate the intrusion of dikes and precipitation of veins; and 3) there is no brittle phase recorded in the quartz diorite, the dikes, the veins, or, most important, the granite mylonite; thus, temperatures in this area must have been elevated for all of the second phase of deformation in order for the granite mylonite to avoid being deformed brittley. The presence of the quartz diorite may well be this reason.

The second phase of deformation is marked by the localized shear zones throughout KFZ, which Sullivan et al. (2013) interpret as recording a transient period of brittle deformation at temperatures between 300 and 350º C. This period of brittle deformation promoted extensive grain-size reduction in most of the Deblois granite close to the center of the KFZ. The grain-size reduction and accompanying phase mixing subsequently catalyzed localized shear zone formation and ultimately the formation of the homogeneous ultramylonites within the main ultramylonite domain (Sullivan et al., 2013). Neither pinstripe ultramylonites described by Sullivan et al. (2013) nor granite mylonites at Fletcher Peak yield any evidence for this brittle phase. Although both pinstripe ultramylonite and granite mylonite were unaffected by the brittle phase, mylonites retain significantly larger quartz recrystallized grain sizes than do pinstripe ultramylonites. While both must have been subjected to prolonged ductile deformation following the initial high-temperature phase of deformation, the granite mylonites do not record as extensive grain-size reduction as pinstripe ultramylonites of Sullivan et al. (2013) do in the third and final phase of deformation in the KFZ. Larger recrystallized grain sizes in the granite

mylonites indicate lower differential stress than the smaller recrystallized grain size observed in the pinstripe ultramylonites (e.g., Hirth and Tullis, 1992; Stipp et al., 2002). A local decrease in differential stress is indicative of a decrease in viscosity at a constant strain rate (Fossen, 2010). This decrease in viscosity could be due to a local increase in temperature or a decrease in grain size.

The third phase of deformation occurred following the development of localized shear zones and was a prolonged period of ductile deformation (Sullivan et al., 2013). During this phase of deformation, the rheology of most of the main ultramylonite domain was governed by the granular flow mechanism (Sullivan et al., 2013). Rocks at Fletcher Peak, however, show little evidence for deformation via granular flow. Pinstripe ultramylonites record later-stage grain size reduction and phase mixing, like the homogeneous ultramylonite; granite mylonite does not. Rather, fluid fugacity, evidenced by the veins promoted deformation by simultaneous dissolution and replacement creep of feldspars, dislocation creep of quartz, and dissolution-precipitation creep of quartz in both granite mylonite and the quartz diorite at Fletcher Peak. All three of these deformation mechanisms are consistent with fluid-assisted deformation at ≥300º C (e.g., Wintsch and Yi, 2002; Wintsch and Yeh, 2013).

7.5 Broader Implications

Studies have shown that ultramylonites develop due to a) grain-size reduction, especially of strong phases (e.g., Stunitz and Fitz Gerald, 1993), or b) chemical alteration to weak phases, especially mica (e.g., Hippert and Hongn, 1998). Sullivan et al. (2013) found that widespread ultramylonites developed in the KFZ due primarily to brittle deformation that led to strain

localization. This study found that the one place at the center of the KFZ where ultramylonite did not develop was due to a lack of brittle processes operating to localize strain, and that where

Stunitz and Fitz Gerald (1993) found that granitoids deformed at low metamorphic grade deformed in two stages based on reducing grain sizes. The dominant deformation mechanism for the second stage was the granular flow of quartz and albite aggregates; superplastic deformation of quartz was secondary. Stunitz and Fitz Gerald (1993) also concluded that feldspar is an important control in rheology when fluids are present; and that granular flow may be more important in controlling rheology than is presently assumed. Mylonites at Fletcher Peak have demonstrated that feldspar is indeed an important factor in rheology, but that without sufficient strain localization and subsequent grain-size reduction, granular flow will not operate.

9. Conclusions

Granite mylonite at Fletcher Peak records two phases of deformation: 1) a high-temperature phase during which quartz underwent grain-boundary-migration recrystallization and feldspars deformed plastically; and 2) a long-lived phase of fluid-assisted deformation, during which feldspar underwent significant dissolution and replacement creep, and quartz deformed by both dissolution-precipitation creep and dislocation creep. The lack of a brittle phase of deformation prevented strain localization and consequent weakening. As a result of the lack of brittle deformation, and due to infiltration of a significant amount of fluid, feldspar and quartz alike deformed via dissolution-precipitation creep rather than by the granular flow that is observed elsewhere in the Deblois granite at the center of the fault line.

References

Bailey, C.M., and Eyster, E.L., 2003, General shear deformation in the Pinaleño Mountains metamorphic core complex, Arizona. Journal of Structural Geology, v. 25, p. 1883-1892.

Bailey, C.M., Simpson, C., and De Paor, D.G., 1993, Volume loss and tectonic flattening strain in granitic mylonites from the Blue Ridge province, central Appalachians. Journal of Structural Geology, v. 16, p. 1403-1416.

Bell, T.H., and Etheridge, M.A., 1973, Microstructure of mylonites and their descriptive terminology. Lithos, v. 6, p. 337-348.

Fossen, H., 2010, Structural Geology: Cambridge University Press, New York, 480 p.

Gerbi, C., and West, D. P., 2007, Use of U-Pb geochronology to identify successive, spatially overlapping tectonic episodes during Silurian-Devonian orogenesis in south-central Maine, USA. Geological Society of America Bulletin, v. 119, p. 1218–1231.

Greene, D.C., and Schweickert, R.A., 1995, The Gem Lake shear zone: Cretaceous dextral transpression in the Northern Ritter Range pendant, eastern Sierra Nevada, California. Tectonics, v. 14, p. 945-961.

Handy, M.R., Hirth, G., and Buergmann, R., 2007, Continental fault structure and rheology from the frictional-to-viscous transition downward, In: Handy, M. R., Hirth, G., Hovius, N. (Eds.), Tectonic faults: Agents of Change on a Dynamic Earth. MIT Press, Cambridge, Mass., USA, p. 139–181.

Hippertt, J.F., and Hongn, F.D., 1998, Deformation mechanisms in the mylonite/ultramylonite transition. Journal of Structural Geology, v. 20, p. 1435-1448.

Hirth, G., and Tullis, J., 1992, Dislocation creep regimes in quartz aggregates. Journal of Structural Geology, v. 14, p. 145–160.

Hubbard, M.S., 1999, Norumbega fault zone: Part of an orogen-parallel strike-slip system, northern Appalachians. In: Ludman, A., and West, D.P., Jr., (eds.), The Norumbega Fault System of the Northern Appalachians. Geological Society of America Special Paper v. 331, p. 155-165.

Killian, R., Heilbronner, R., and Stünitz, H., 2011, Quartz grain size reduction in a granitoid rock and the transition from dislocation to diffusion creep. Journal of Structural Geology, v. 33, p. 1265-1284.

Ludman, A., Lanzirotti, A., Lux, D., Wang, C., 1999, Constraints on timing and displacement of multiple shearing in the Norumbega fault system, eastern Maine, in: Ludman, A., West, D.P. Jr., (eds.), The Norumbega Fault System of the Northern Appalachians, Geological Society of America Special Paper, v. 331, p. 179–194.

Ludman, A., Wang, C., Gibbons, S., Idleman, B., Rasbury, T., 2000, Geometry and timing of multiple faulting events in the Kellyland fault zone (Norumbega fault system) in the Fletcher Peak-Wabassus Mountain area, eastern Maine. In: Yates, M., Lux, D., Kelley, J. (eds.) Guidebook for Field Trips in Coastal and East-Central Maine. Guidebook-New England Intercollegiate Geological Conference, v. 92, p. 1-22.

Ludman, A. and West, D.P. Jr., (eds.), 1999, The Norumbega Fault System of the Northern Appalachians. Geological Society of America Special Paper, v. 331, p. v–xii.

Menegon, L., Pennacchioni, G., Spiess, R., 2008, Dissolution-precipitation creep of K-feldspar

in mid-crustal granite mylonites. Journal of Structural Geology, v. 30, p. 565-579.
O'Hara, K., 1988. Fluid flow and volume loss during mylonitization: an origin for phyllonite in an overthrust setting, North Carolina, U.S.A. Tectonophysics, v. 156, p. 21–36.
Passchier, C.W., 1982, Mylonitic deformation in the Saint-Barthélemy Massif, French Pyrenees, with emphasis on the genetic relationship between ultramylonite and pseudotachylite. GUA Papers of Geology, v.1, p. 16:1-173.
Passchier, C.W., and Trouw, R.A.J., 2005, Microtectonics: Springer, Berlin, 366 p.
Peternell, M., Hasalová, P., Wilson, C.J.L., Piazolo, S., and Schulammn, K., 2010, Evaluating quartz crystallographic preferred orientations and the role of deformation partitioning using EBSD and fabric analyser techniques. Journal of Structural Geology, v. 32, p. 803-817.
Platt, J.P., and Behr, W.M., 2011. Grain size evolution in ductile shear zones: implications for strain localization and the strength of the lithosphere. Journal of Structural Geology, v. 33, p. 537-550.
Price, N.A., Johnson, S.E., Gerbi, C.C., and West, D.P., Jr., 2012, Identifying deformed pseudotachylite and its influence on the strength and evolution of a crustal shear zone at the base of the seismogenic zone. Tectonophysics, 518-521, p. 63-83.
Riley, D.N., 2004, Granites, orogeny, and the Deblois pluton complex in eastern Maine, USA. Ph.D. dissertation, Ohio State University, 546 p.
Schmid, S.M., and Casey, M., 1986, Complete fabric analysis of some commonly observed quartz c-axis patterns. Geophysical Monograph, v. 36, p. 263-286.
Sibson, R.H., 1977, Fault rocks and fault mechanisms. Journal of the Geological Society of London, v. 133, p. 191-213.
Snoke, A., Tullis, J., and Todd, V.R., 1998, Fault-related rocks: a photographic atlas. Princeton University Press: Princeton, 617 p.
Stipp, M., Stunitz, H., Heilbronner, R., Schmid, S.M., 2002, The eastern Tonale fault zone: a 'natural laboratory' for crystal plastic deformation of quartz over a temperature range from 250 to 700°C. Journal of Structural Geology, v. 24, 1861-1884.
Stipp, M., and Tullis, J., 2003, The recrystallized grain size piezometer for quartz. Geophysical Research Letters, doi:10.1029/2003GL018444.
Stunitz, H., and Fitz Gerald, J.D., 1993, Deformation of granitoids at low metamorphic grade II: granular flow in albite-rich mylonites. Tectonophysics, v. 221, p. 299-324.
Sullivan, W.A., and Beane, R.J., 2010, Asymmetrical quartz crystallographic fabrics formed during constrictional deformation. Journal of Structural Geology, v. 32, p. 1430-1443.
Sullivan, W.A., Boyd, A.S., and Monz, M.E., 2013, Strain localization in homogeneous granite near the brittle-ductile transition: A case study of the Kellyland fault zone, Maine, USA. Journal of Structural Geology, v. 56, p. 70-88.
Trouw, R.A.J., Passchier, C.W., and Wiersma, D.J., 2009, Atlas of Mylonites- and related microstructures: Springer, Berlin, 322 p.
Tullis, J., 2002, Deformation of granitic rocks: experimental studies and natural examples. In: Karato, S., Wenk, H., (eds.), Plastic Deformation of Minerals and Rocks, Reviews in Mineralogy and Geochemistry, v. 51, p. 51-95.
Tullis, J., and Yund, R.A., 1985, Dynamic recrystallization of feldspar: A mechanism for ductile shear zone formation. Geology, v. 13, p. 238-241.
Tullis, J., Yund, R.A., 1987, Transition from cataclastic flow to dislocation creep of feldspar: Mechanisms and microstructures. Geology, v. 15, p. 606-609.
Wang, C., and Ludman, A., 2004, Deformation conditions, kinematics, and displacement history

of shallow crustal ductile shearing in the Norumbega fault system in the Northern Appalachians, eastern Maine. Tectonophysics, v. 384, p. 129–148.

Wintsch, R.P., and Yeh, M., 2013, Oscillating brittle and viscous behavior through the earthquake cycle in the Red River Shear Zone: Monitoring flips between reaction and textural softening and hardening. Tectonophysics, v. 587, p. 46-62.s

Wintsch, R.P., and Yi, K., 2002, Dissolution and replacement creep: a significant deformation mechanism in mid-crustal rocks. Journal of Structural Geology, v. 24, p. 1179-1193.

Figure captions

1. A) Simplified map showing major strike-slip faults and plutons throughout Maine. B) Geologic map of eastern Maine and adjacent New Brunswick showing extent of the Kellyland fault zone (KFZ). The Codyville fault zone (CFZ) and Waite fault zone (WFZ) are also shown. Deblois granite (DG) is delineated, and area of Figure 2 is outlined. From Sullivan et al. (2013).
2. A) Map of the Kellyland fault zone in the Machias Lakes area showing strain facies in Deblois granite and metasedimentary rocks. B) Map showing extent of Fletcher Peak study area, and known extent of granitic mylonite within the main ultramylonite domain. Numbers represent locations where samples were collected.
3. Simplified depiction of band of mylonite sandwiched between ultramylonite zones within the main ultramylonite domain within the Deblois granite cut by the KFZ.
4. Photo of sawn block of undeformed Deblois granite from Sullivan et al., 2013.
5. Equal area, lower-hemisphere projection showing poles to foliation from all lithologies at Fletcher Peak. Pink are foliation measurements of granite mylonite; blue are lineation measurements of granite mylonite; green are foliation measurements of quartz diorite; gray are foliation measurements of quartz veins.
6. Photographs of sawn blocks of granitic mylonites from Fletcher Peak. These samples transverse the KFZ across-strike from FP03-A as the farthest from the center of the zone, to FP01 as the closest to the center of the zone. Sample locations given in Figure 2B. FP01 is a granitic mylonite closest to the granitic mylonite-quartz diorite contact. Sample FP02-E is a granitic mylonite at site adjacent to figure 6A. Sample FP03-A is a granite mylonite adjacent to figure 6B. Photographs by W.A. Sullivan (2012).

7. Photographs of dikes and veins at Fletcher Peak. A) Leucogranite dike in granitic mylonite. B) Quartz vein in granitic mylonite. Note small leucogranite dike at top right. C) Quartz vein and associated leucogranite dike in granitic mylonite.
8. Isocon plots of major-element compositions of granite mylonite samples vs. average granite composition from Sullivan et al. (2013). See Table 3 for data used to make these plots.
9. Cross-polarized light micrographs showing microstructures of feldspars in granitic mylonites at Fletcher Peak. Sample numbers are in right-hand corner of each image. See Figure 2B for sample locations. A) Partially recrystallized perthitic microcline. B) Micrograph showing contrasting microstrcuture of microcline (center of image) and plagioclase feldspar (periphery of image). C) Partially recrystallized microcline ribbon surrounded by hornblende and biotite. D) Bookshelf-type fracturing along cleavage planes in plagioclase feldspar and composite ribbon of relict microcline grains and neoblasts. E) Plagioclase grain with myrmekitic intergrowth of quartz and k-feldspar at high-strain site. F) Partially recrystallized perthitic microcline grain with quartz pressure-shadow wings and quartz growing in dilatational site in center of image. G) Dilatational fractures in microcline filled by k-feldspar.
10. Cross-polarized light micrographs of quartz in granitic mylonite from Fletcher Peak. Sample numbers located in right-hand corner of each image. See Figure 2B for sample locations. A) Quartz ribbon with partially recrystallized feldspar porphyroclasts. Note two ‘classes’ of recrystallized quartz grains: larger amoeboid grains, and smaller subgrains and neoblasts. Also note replacement of feldspar by quartz in both feldspar clasts. B) Quartz ribbon showing two clear classes of recrystallized grains.

11. Transmitted-light micrographs of hornblende in granitic mylonites. Sample numbers located in right-hand corner of each image. See Figure 2B for sample locations. A-B) Pair of images of same field of view showing partial actinolite replacement in hornblende porphyroclast. 8A was taken in plane-polarized light and 8B was taken in cross-polarized light. Note apatite inclusions in hornblende, visible in the center of image 8A. C) Hornblende porphyroclast with biotite wing and partial biotite replacement.
12. Cross-polarized light micrographs of plagioclase, microcline and quartz in quartz-diorite at Fletcher Peak. Sample numbers located in right-hand corner of each image. See Figure 2B for sample locations. A) Plagioclase grains exhibiting dilatational fractures filled with quartz and quartz pressure-shadow wings. B) Plagioclase feldspars with abundant dilatational fractures and quartz pressure-shadow wings, surrounded by other mineral phases. C) Microcline porphyroclast with dilatational fractures into which quartz has precipitated.
13. Cross-polarized light micrograph showing compositional heterogeneity in quartz-diorite at Fletcher Peak.
14. Cross-polarized light micrograph showing foliation in aplitic leucogranite dike defined by mica bands and alteration products of micas.
15. Cross-polarized light micrographs of feldspars in leucogranite dikes. Sample numbers located in right-hand corner of each image. See Figure 2B for sample locations. A) Microcline porphyroclast with minor perthite (center), quartz pressure-shadow wings, and replacement by quartz at high-strain sites. Also note dilatant site at center of grain into which quartz has precipitated. B) Microcline replaced with quartz. Note also quartz in high-strain site at bottom right of microcline. C) Myrmekite in plagioclase feldspar. D)

Microcline porphyroclast with significant replacement by quartz, quartz pressure-shadow overgrowths, and quartz precipitaion into seams of the porphyroclast. E) Microcline grain with tails of neoblsts, a biotite solution seam at bottom, and flame perthite development at high-stress sites.

16. Cross-polarized light micrograph of interspersed recrystallized quartz grains and feldspar neoblasts in leucogranite dike. Sample collected at station FP09 (Fig. 2B).
17. Cross-polarized light micrographs of muscovite fish in leucogranite dikes. Sample numbers located in right-hand corner of each image. See Figure 2B for sample locations. A) Muscovite fish in mylonitic aplite dike. B) Muscovite fish in dike, split along basal plane. C) Muscovite fish split along fold hinge.
18. Cross-polarized light micrographs of quartz vein hosted in quartz-diorite. A) Recrystallized quartz grains and subgrains in quartz vein, cross-polarized light. B) Same area as A, but with 1/λ retardation plate inserted.
19. Equal-area, lower-hemisphere projections of quartz crystallographic fabrics measured in rocks from Fletcher Peak. See Figure 2B for sample locations. A) Contoured lattice-preferred orientation pattern of c-axes (left) and a-axes (right) in quartz vein hosted in quartz diorite. Collected at station FP07. B) Contoured lattice-preferred orientation pattern of c-axes (left) and a-axes (right) in quartz ribbon in granite mylonite sample FP03-A.
20. Diagram illustrating strain shadows on feldspar porphyroclast. From Fossen, 2010.

Table 1

Station locations in UTM. All located in zone 19.

Station	East	North	Lithology
FP01	581212	4993129	Granite mylonite
FP02	581309	4993126	Granite mylonite
FP03	581387	4993108	Granite mylonite and quartz vein
FP07	581119	4993434	Quartz diorite and quartz vein
FP09	581142	4993311	Leucogranite dike

Table 2
Major element concentrations in weight percent.*

Sample	SiO2	Al2O3	Fe2O3(T)	MnO	MgO	CaO	Na2O	K2O	TiO2	P2O5	LOI
Protolith											
Undeformed granite											
KL51	70.54	14.04	3	0.04	0.32	1.47	3.61	5.12	0.34	0.02	0.84
KL42	72.32	13.2	3.55	0.05	0.3	1.33	3.15	5.58	0.367	0.09	0.33
Foliated granite											
KL44	73.07	13.35	3.02	0.04	0.24	1.15	3.04	5.44	0.316	0.05	0.83
KL01	73.33	13.14	3.38	0.05	0.29	1.3	2.95	5.3	0.373	0.06	0.67
KL40-78	70.47	13.78	3.31	0.05	0.26	1.46	3.2	5.32	0.348	0.07	0.81
Average granite	71.95	13.5	3.25	0.05	0.29	1.35	3.19	5.35	0.35	0.06	0.712
Granite mylonite											
FP01	65.3	14.65	6.06	0.11	0.46	2.45	3.47	5.66	0.607	0.16	0.89
FP03-A	69.2	13.92	4.17	0.07	0.37	1.42	3.27	5.4	0.453	0.13	0.74
KL21	59.97	16.5	8.81	0.16	0.73	3.02	3.88	5.11	0.927	0.27	1.27

* Analytical errors are ±0.01% for Si, Al, Fe, Mn, Mg, Ca, Na, K, P, and LOI; ±0.05% for Ti.

Table 3

Trace element concentrations in PPM.*

Sample	Hf	Tb	Yb	Lu	Sc	Cr	Ni	Rb	Sr	U	Th	Cs	V	Y	Zr
Protolith															
Undeformed granite															
KL51	7.2	0.9	3.6	0.59	5.5	16	5	250	103	3.2	6	8.9	22	34	262
KL42	8.3	1.4	4.2	0.66	6.5	14	7	230	84	4.2	12.1	8.3	20	43	365
Foliated granite															
KL40-78	8.8	1.4	4.8	0.71	7	17	6	200	86	2.5	16.5	4.3	20	50	356
KL01	9.4	1.2	4.6	0.73	7.8	19	7	220	84	3.2	13.6	6.9	22	46	351
Average granite	8.4	1.1	4.2	0.7	6.5	16.4	5.8	224	91	4.2	12.6	7.3	20.8	40.2	532.2
Granite mylonite															
KL21	18.6	1.5	5.7	0.94	15.9	10	8	140	196	2.5	4.5	10.1	30	58	942
KL22-A	7.6	1.2	3.9	0.62	6.8	8	5	180	113	3.5	8.1	7.3	18	42	358
KL28	13.1	2.1	5.8	0.95	11.9	< 1	7	120	137	4.4	9.9	6.8	17	59	563

* Analytical errors are ±20 PPM for V; ±4 PPM for Zr; ±1 PPM for Cr, Ni, and Y; ±500 PPB for Cs, Hf, Tb, Th, and U; ±500 PPB for Sr; ±100 PPB for Sc and Yb; ±50 PPB for Lu.

Table 4

XRD analyses of major phases in granite mylonites and quartz diorite.

Sample (weight %)	Quartz	Feldspar	Biotite	Hornblende	Tremolite
Granite mylonite					
FP01	24.3	66.3	1.3	8.6	
FP02-E	18.6	69.1	8	5.8	
FP03	33.9	63.75	2.01	0.4	
Quartz diorite					
FP07-A	17.5	50.3	3.8	21.5	7

Table 5

Two-dimensional quartz recrystallized grain size in µm.

Rock type	Granite mylonite				Quartz diorite
Sample	FP01	FP02-E	FP03-A	Average	FP07-A
Max	52.2	102.755	60.3	71.75	82.5
Min	5.34	7.395	6.7	6.48	9.325
Mean	14.97	25.02	22.5	20.83	36.61
Median	13.805	17.605	19.8	17.07	23.88
Std dev	6.18	18.96	11.1	12.08	24.54

Figure 1.

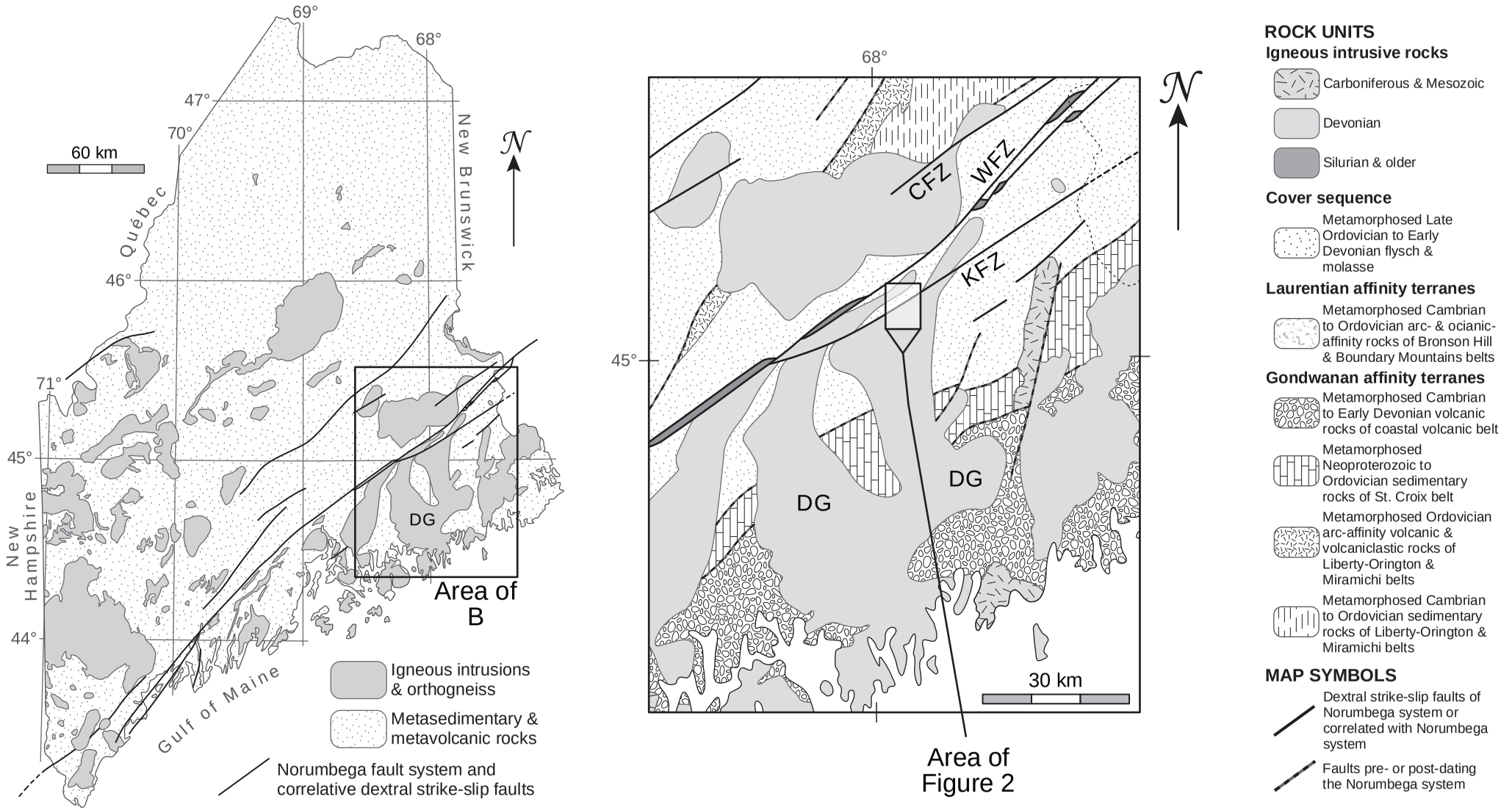
69°
68°
47°
70°
60 km
Québec
New Brunswick
N
46°
71°
45°
New Hampshire
DG
Area of B
44°
Gulf of Maine
Igneous intrusions & orthogneiss
Metasedimentary & metavolcanic rocks
Norumbega fault system and correlative dextral strike-slip faults
68°
CFZ
WFZ
KFZ
N
45°
DG
DG
30 km
Area of Figure 2
ROCK UNITS
Igneous intrusive rocks
Carboniferous & Mesozoic
Devonian
Silurian & older
Cover sequence
Metamorphosed Late Ordovician to Early Devonian flysch & molasse
Laurentian affinity terranes
Metamorphosed Cambrian to Ordovician arc- & ocianic-affinity rocks of Bronson Hill & Boundary Mountains belts
Gondwanan affinity terranes
Metamorphosed Cambrian to Early Devonian volcanic rocks of coastal volcanic belt
Metamorphosed Neoproterozoic to Ordovician sedimentary rocks of St. Croix belt
Metamorphosed Ordovician arc-affinity volcanic & volcaniclastic rocks of Liberty-Orington & Miramichi belts
Metamorphosed Cambrian to Ordovician sedimentary rocks of Liberty-Orington & Miramichi belts
MAP SYMBOLS
Dextral strike-slip faults of Norumbega system or correlated with Norumbega system
Faults pre- or post-dating the Norumbega system

Figure 2.

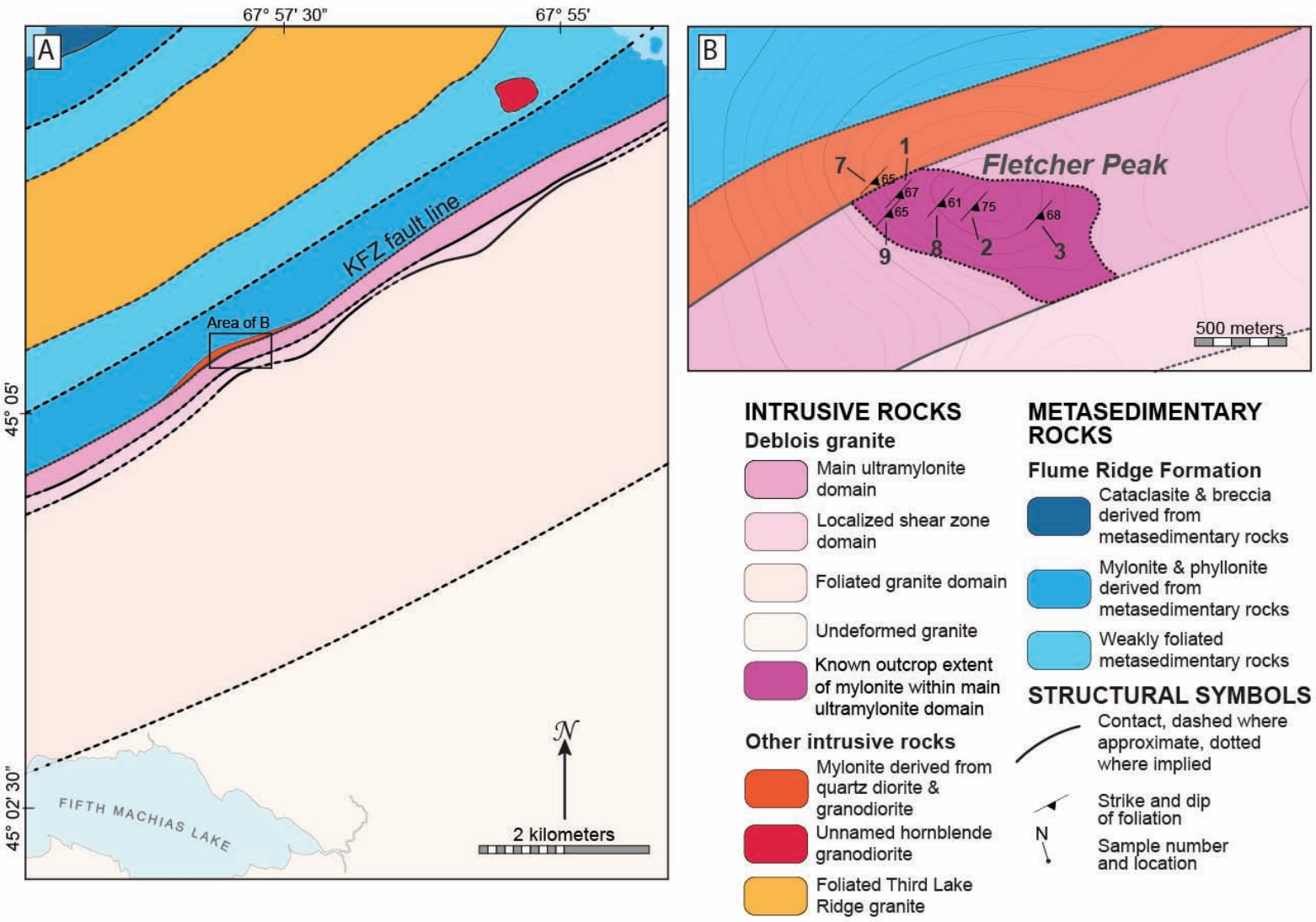
A
67° 57' 30"
67° 55'
45° 05'
45° 02' 30"
KFZ fault line
Area of B
FIFTH MACHIAS LAKE
N
2 kilometers
B
Fletcher Peak
1
2
3
7
8
9
65
67
65
61
75
68
500 meters
INTRUSIVE ROCKS
Deblois granite
Main ultramylonite domain
Localized shear zone domain
Foliated granite domain
Undeformed granite
Known outcrop extent of mylonite within main ultramylonite domain
Other intrusive rocks
Mylonite derived from quartz diorite & granodiorite
Unnamed hornblende granodiorite
Foliated Third Lake Ridge granite
METASEDIMENTARY ROCKS
Flume Ridge Formation
Cataclasite & breccia derived from metasedimentary rocks
Mylonite & phyllonite derived from metasedimentary rocks
Weakly foliated metasedimentary rocks
STRUCTURAL SYMBOLS
Contact, dashed where approximate, dotted where implied
Strike and dip of foliation
N
Sample number and location

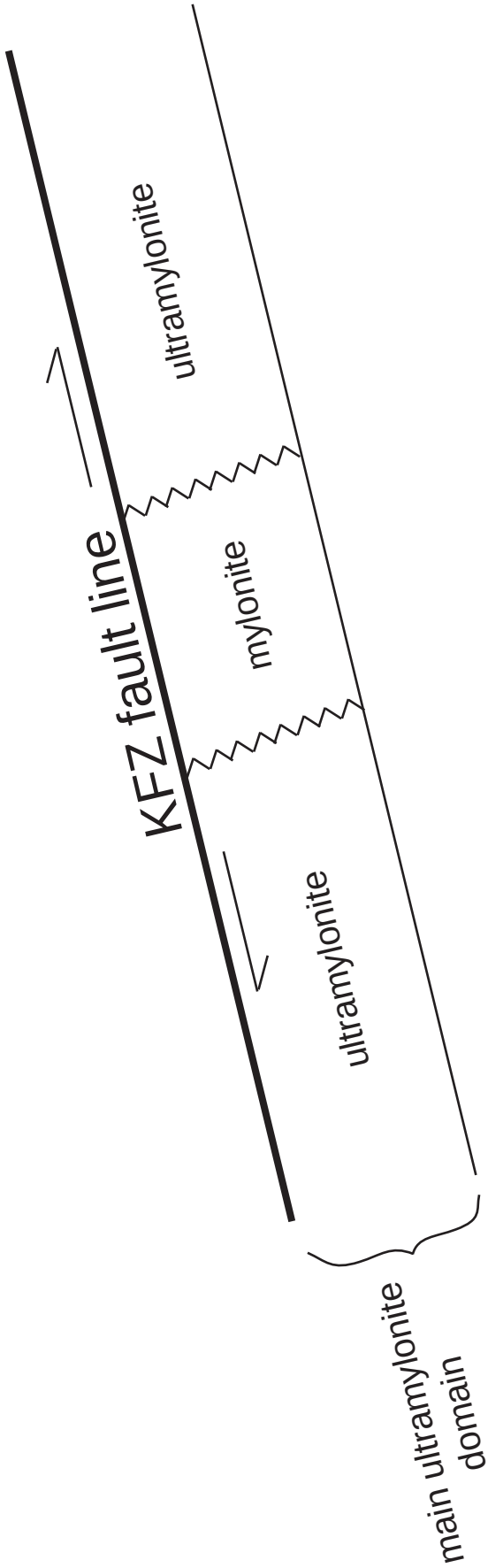
KFZ fault line
ultramylonite
mylonite
ultramylonite
main ultramylonite domain

Figure 3.

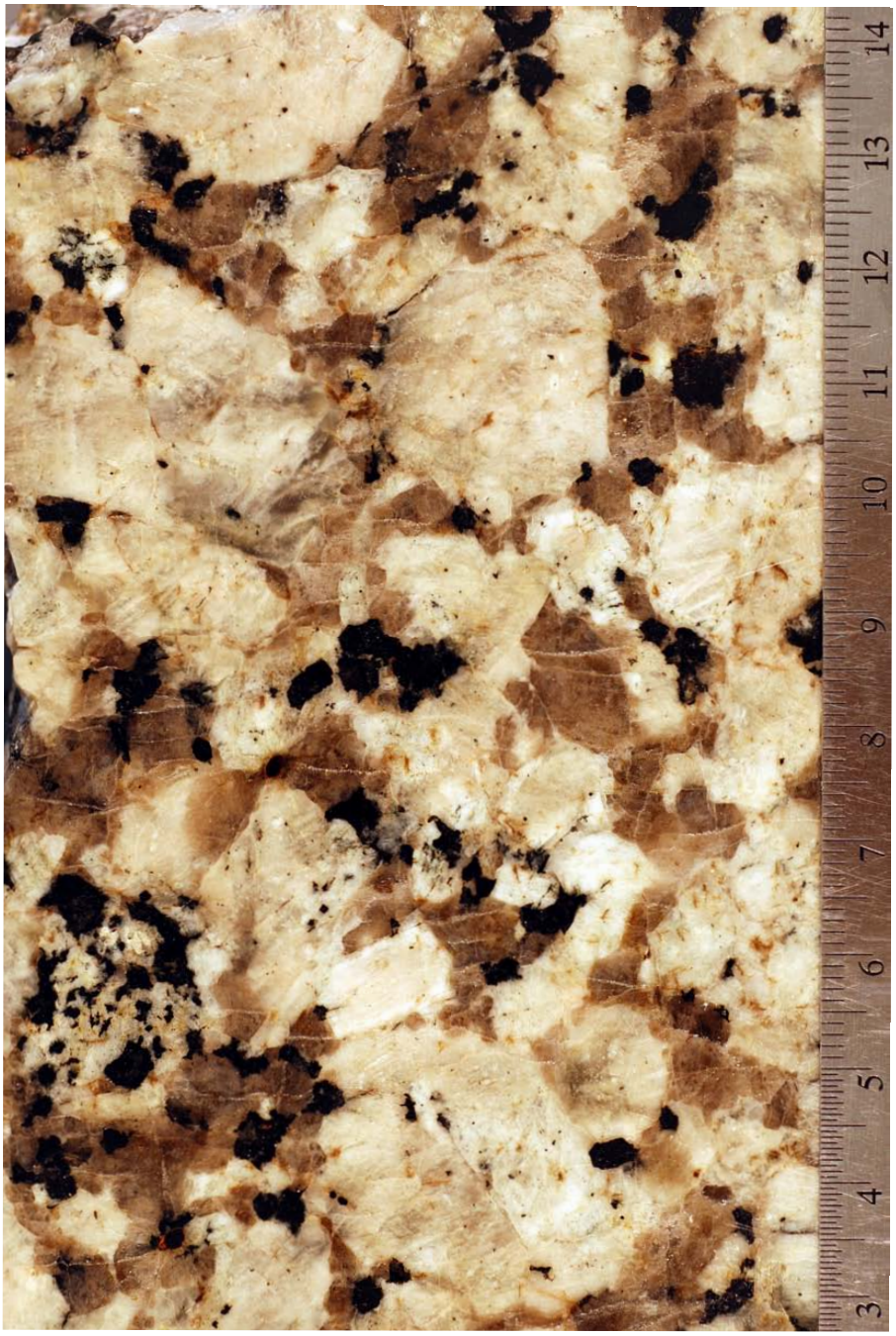

Figure 4.

Figure 5.

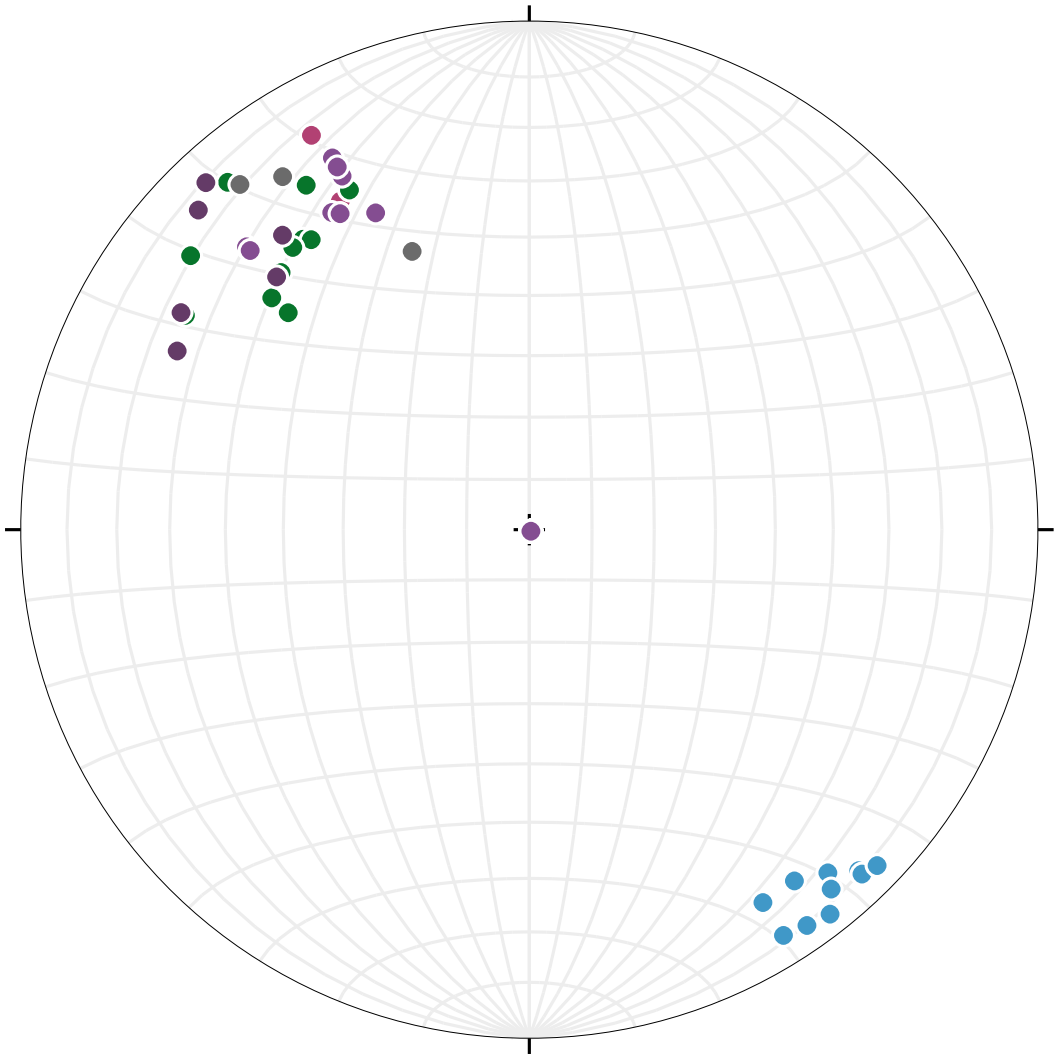

Figure 6.

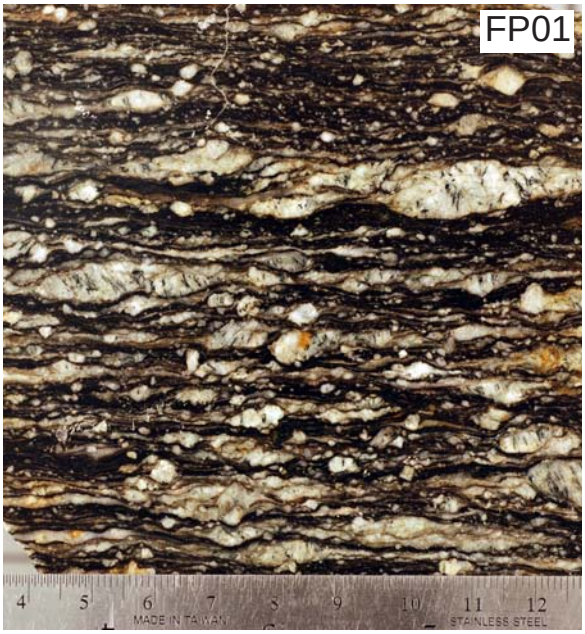
FP01
MADE IN TAIWAN
STAINLESS STEEL


FP02-E
MADE IN TAIWAN
STAINLESS STEEL

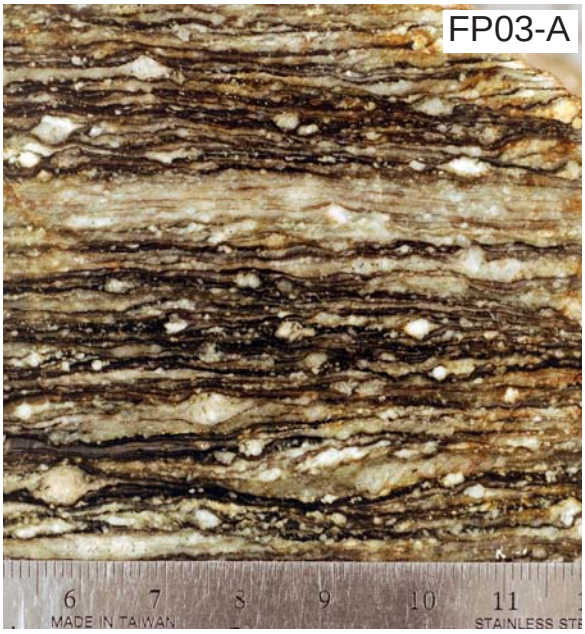
FP03-A
MADE IN TAIWAN

Figure 7.

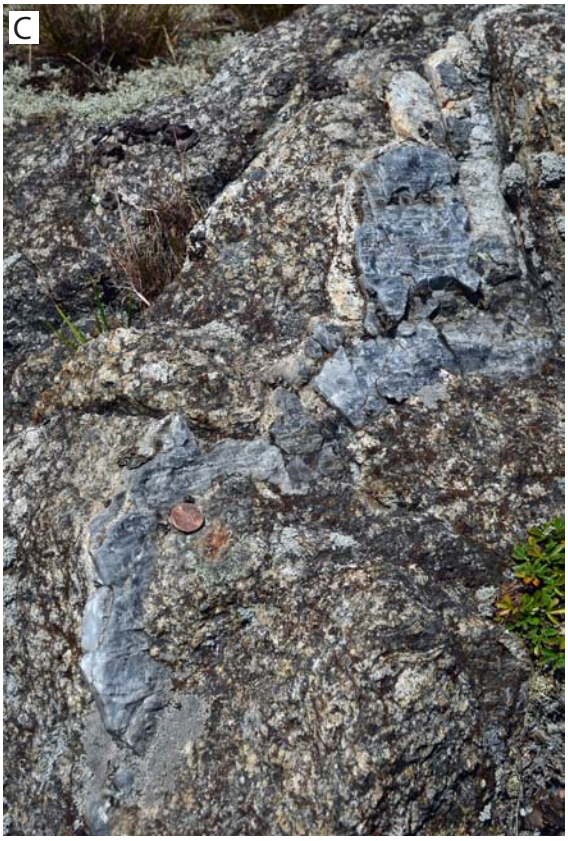

Figure 8.

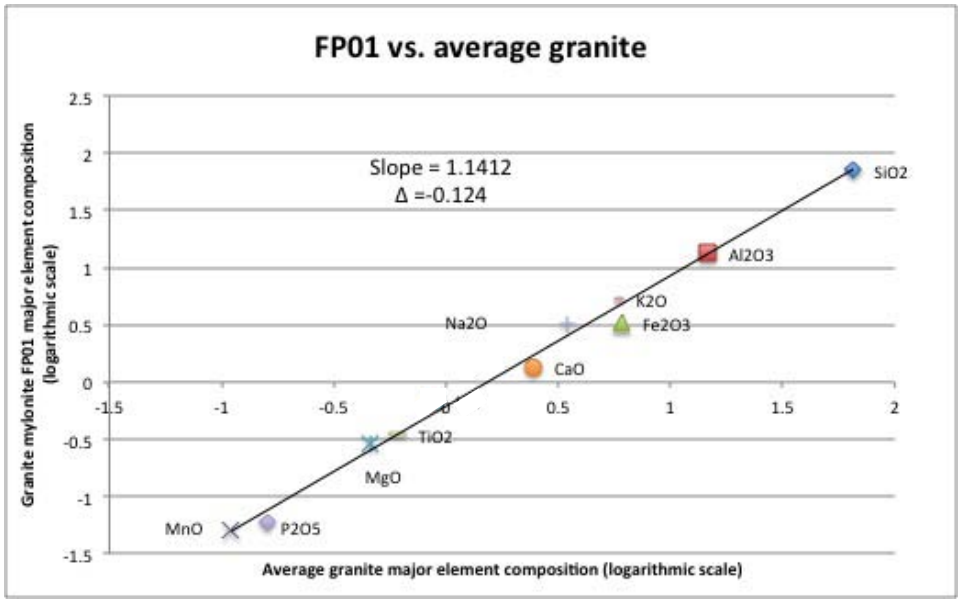
FP01 vs. average granite
Slope = 1.1412
Δ =-0.124
Granite mylonite FP01 major element composition (logarithmic scale)
Average granite major element composition (logarithmic scale)
SiO2
Al2O3
K2O
Na2O
Fe2O3
CaO
TiO2
MgO
MnO
P2O5

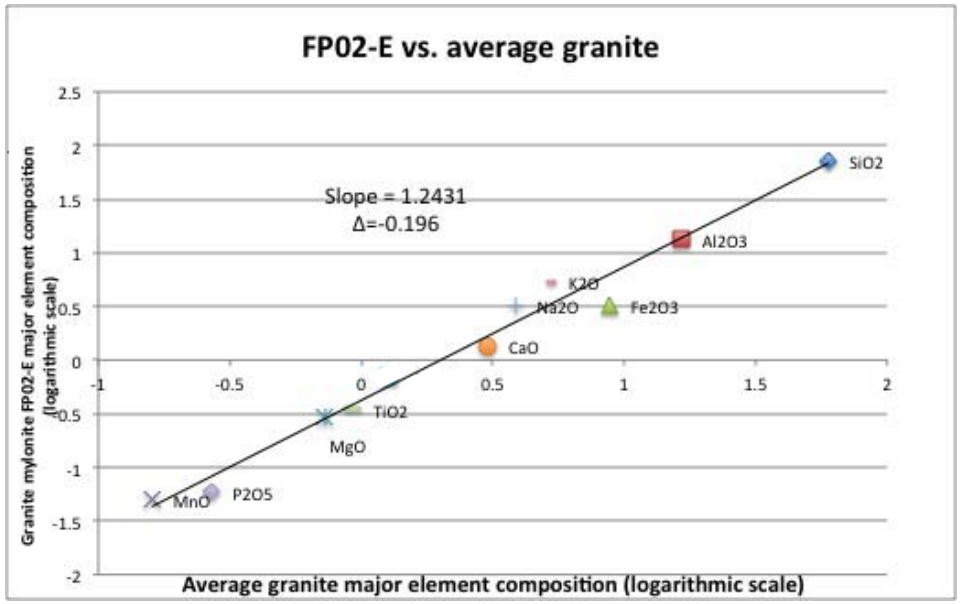
FP02-E vs. average granite
Slope = 1.2431
Δ=-0.196
Granite mylonite FP02-E major element composition (logarithmic scale)
Average granite major element composition (logarithmic scale)
SiO2
Al2O3
K2O
Na2O
Fe2O3
CaO
TiO2
MgO
MnO
P2O5

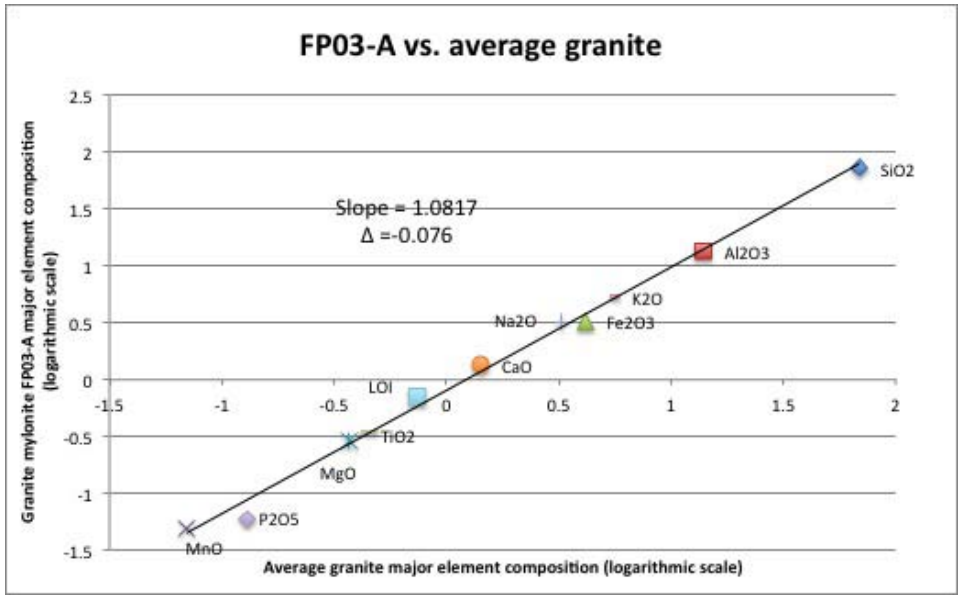
FP03-A vs. average granite
Slope = 1.0817
Δ =-0.076
Granite mylonite FP03-A major element composition (logarithmic scale)
Average granite major element composition (logarithmic scale)
SiO2
Al2O3
K2O
Na2O
Fe2O3
CaO
LOI
TiO2
MgO
P2O5
MnO

Figure 9.

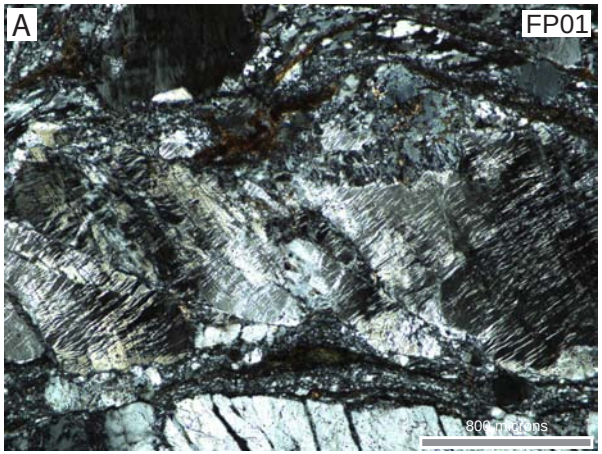
A
FP01
800 microns

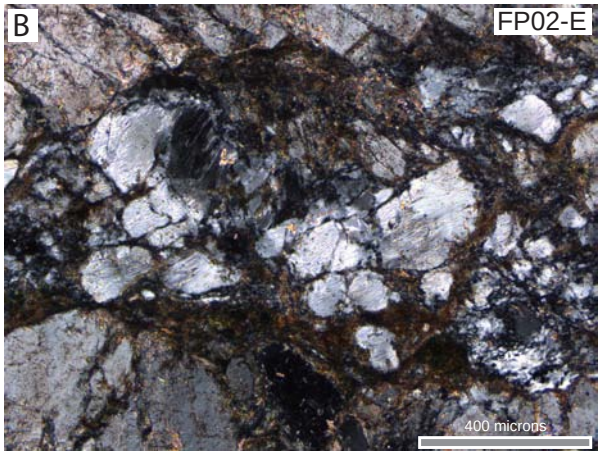
B
FP02-E
400 microns

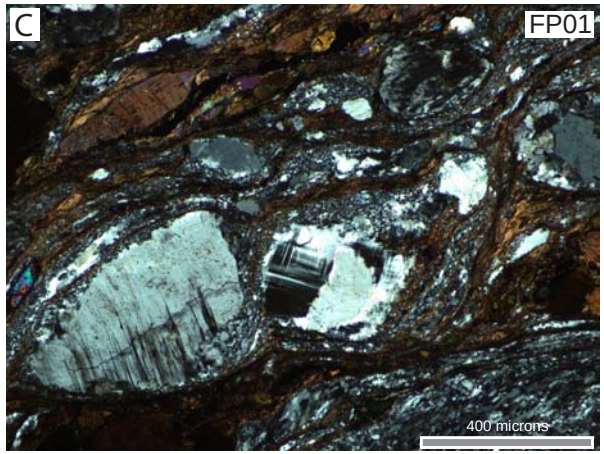
C
FP01
400 microns

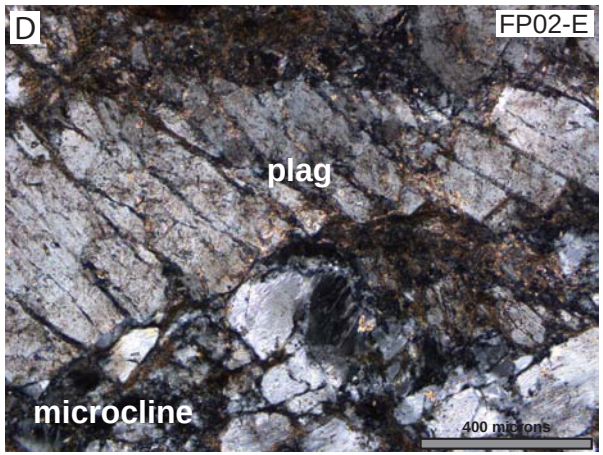
D
FP02-E
plag
microcline
400 microns

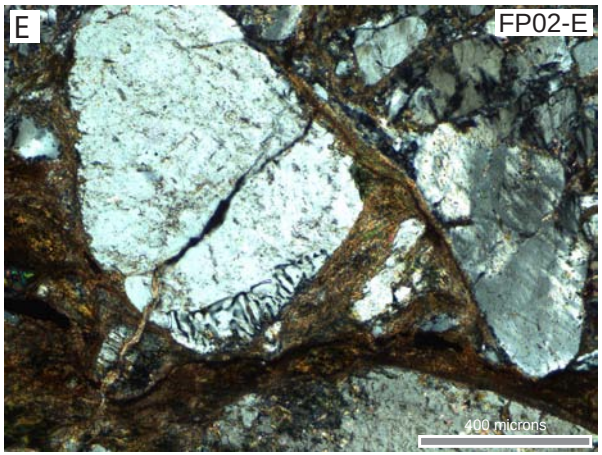
E
FP02-E
400 microns

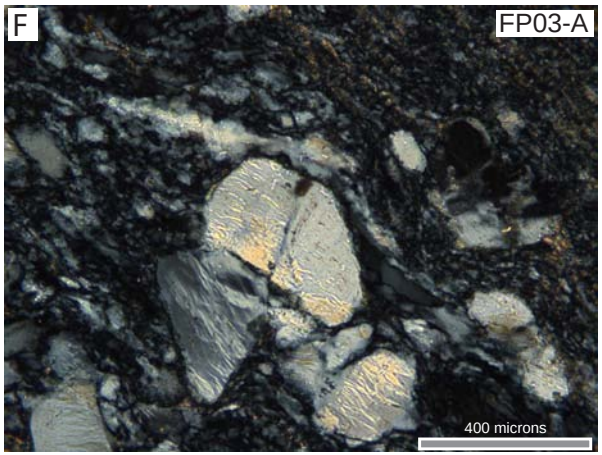
F
FP03-A
400 microns

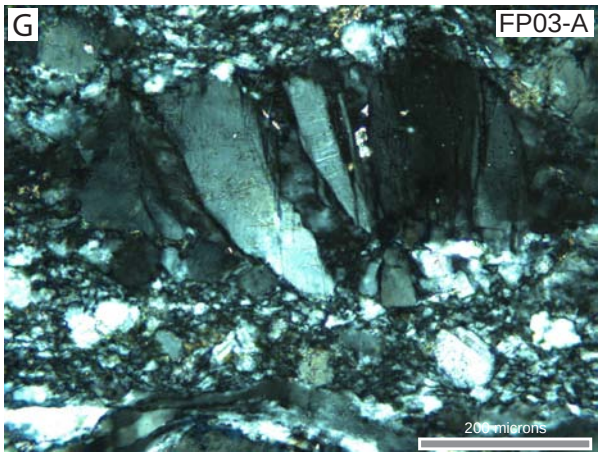
G
FP03-A
200 microns

Figure 10.

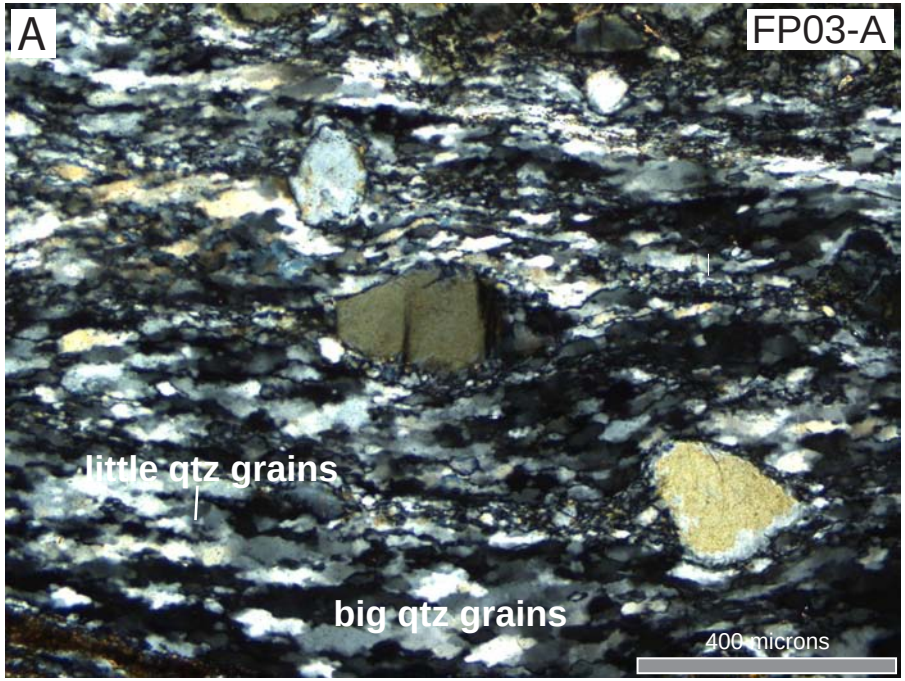
A
FP03-A
little qtz grains
big qtz grains
400 microns

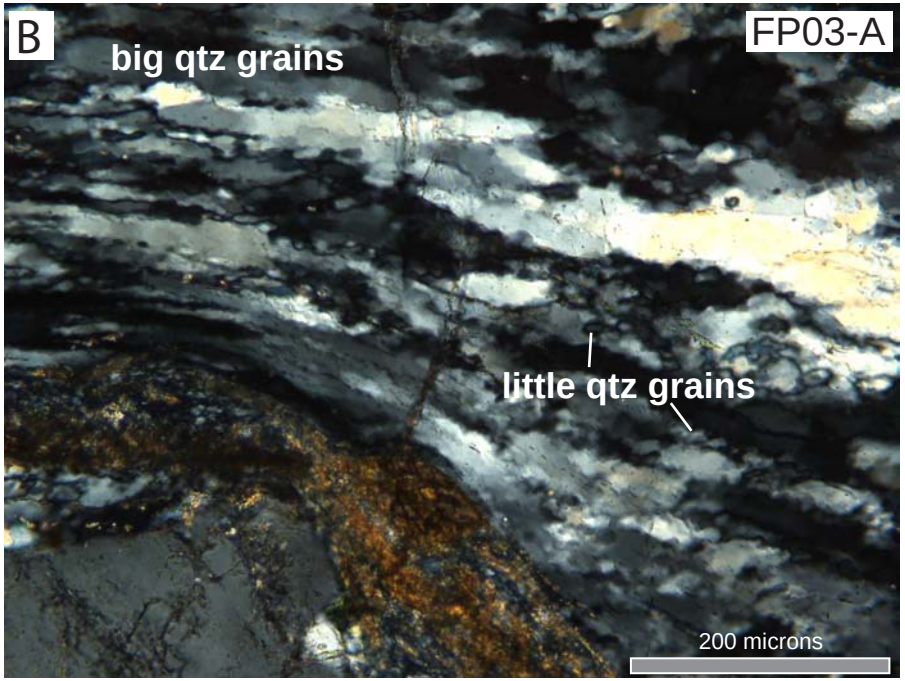
B
big qtz grains
FP03-A
little qtz grains
200 microns

Figure 11.

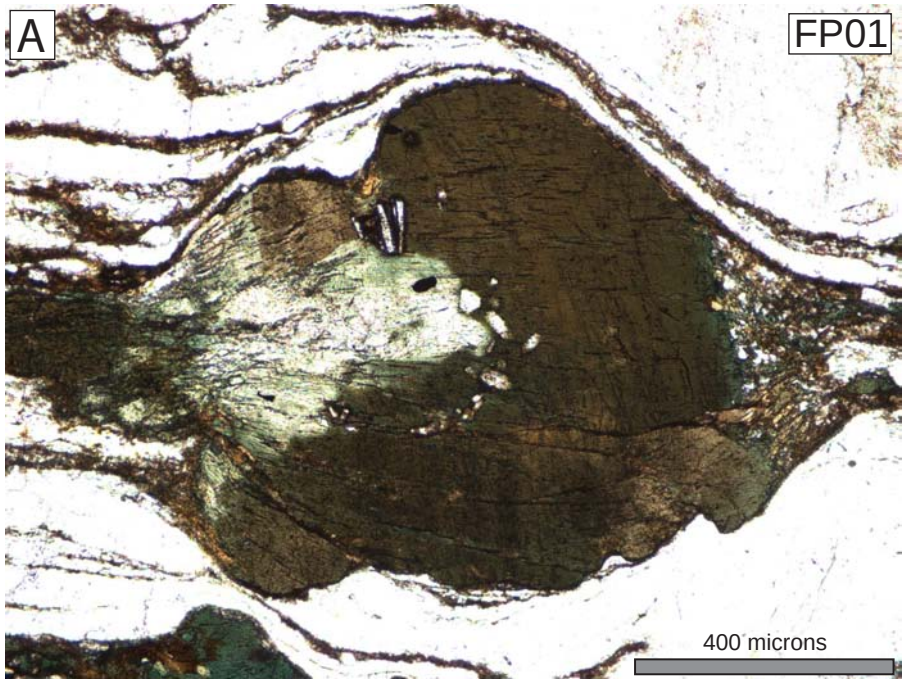

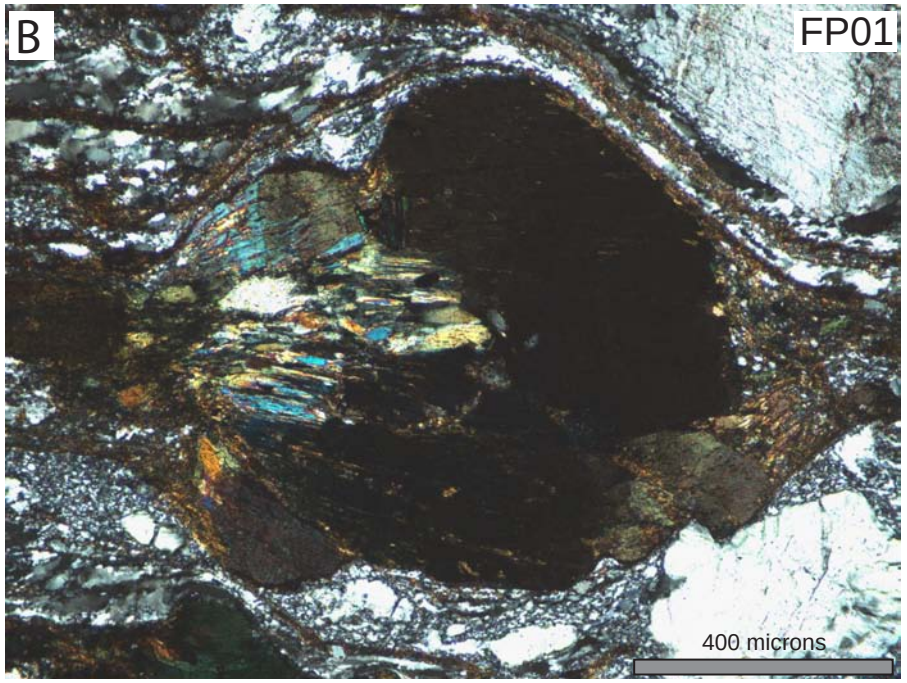

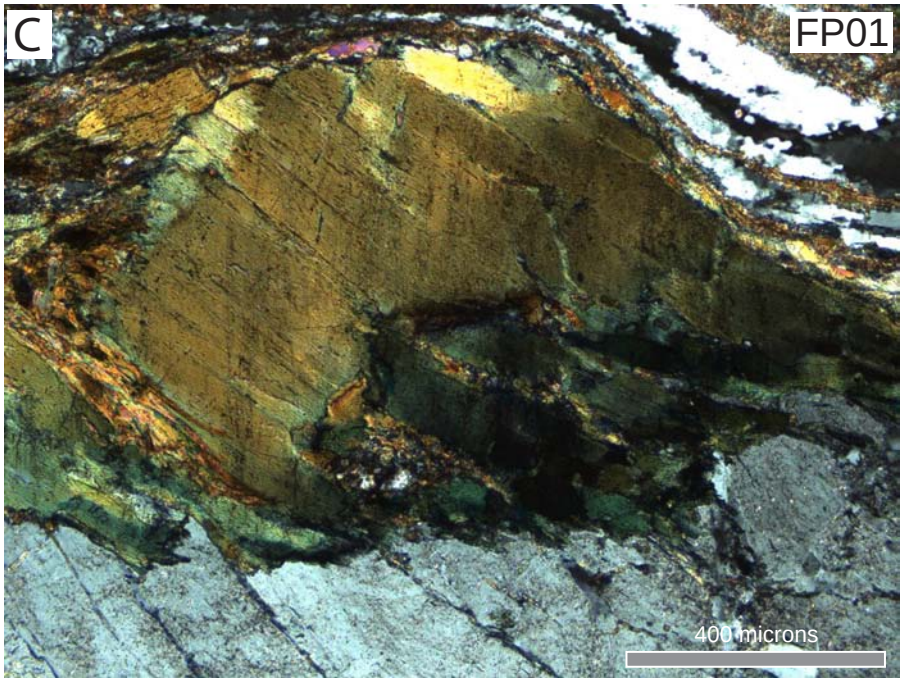

Figure 12.

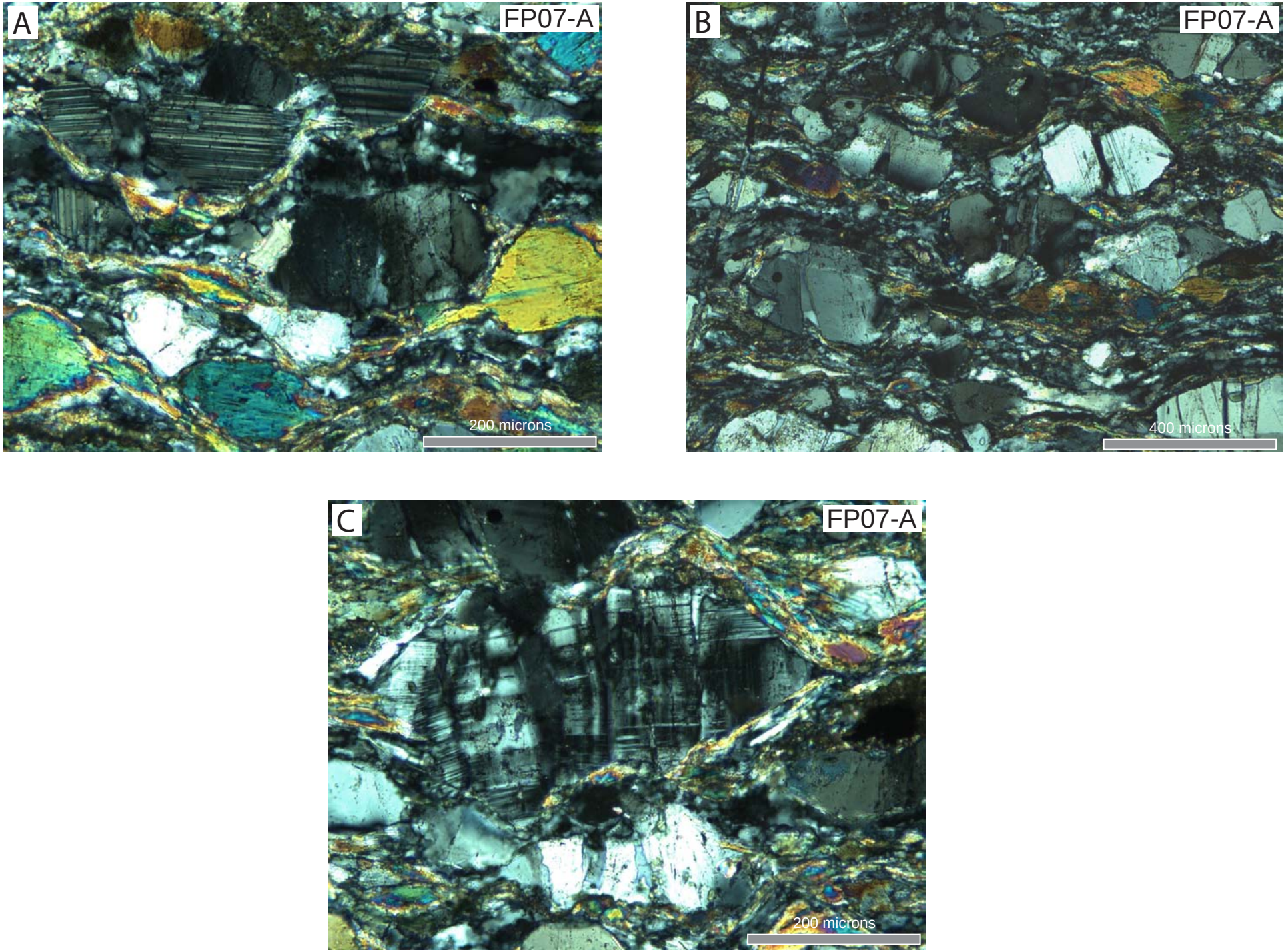

Figure 13.

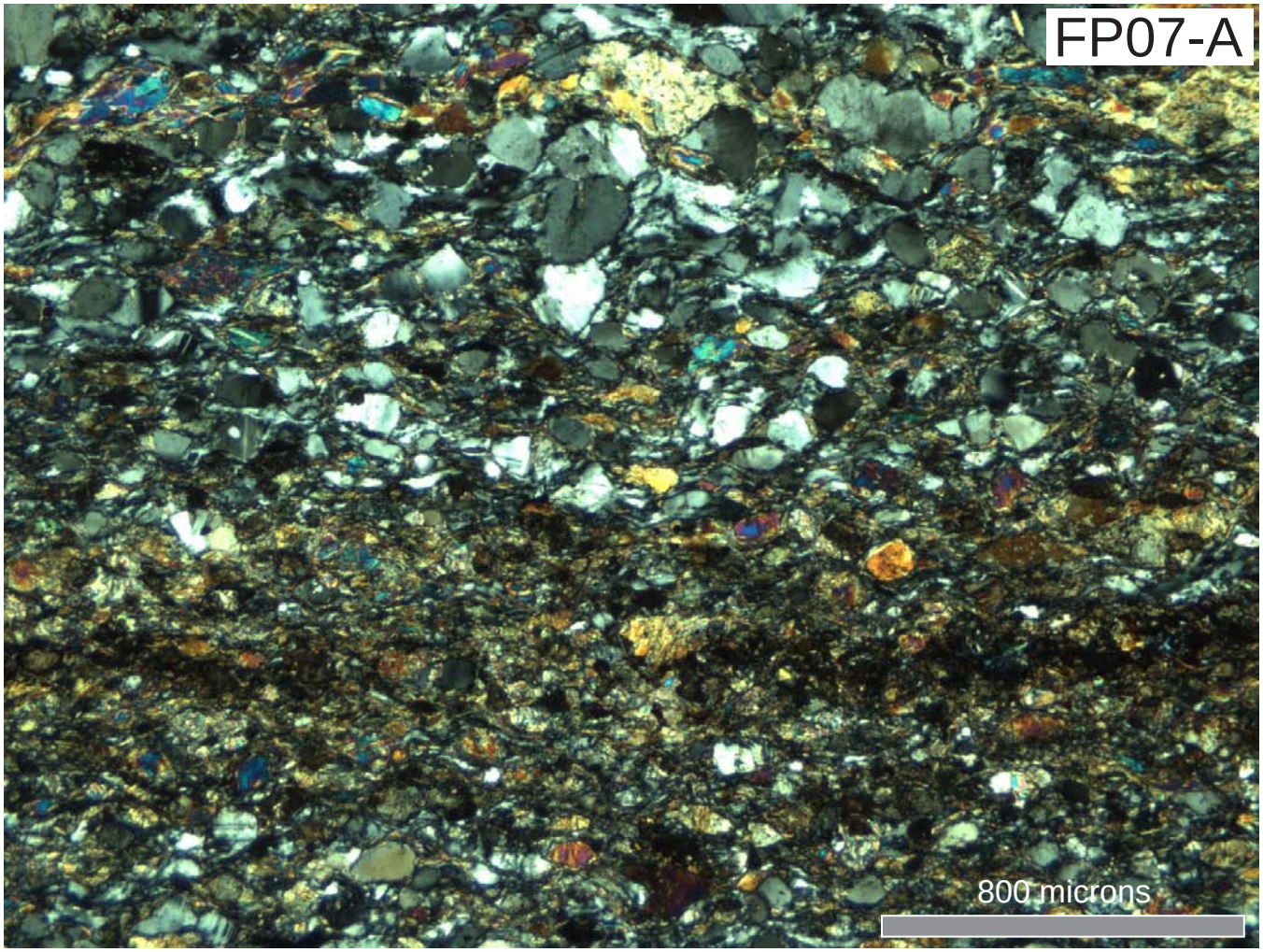

Figure 14.

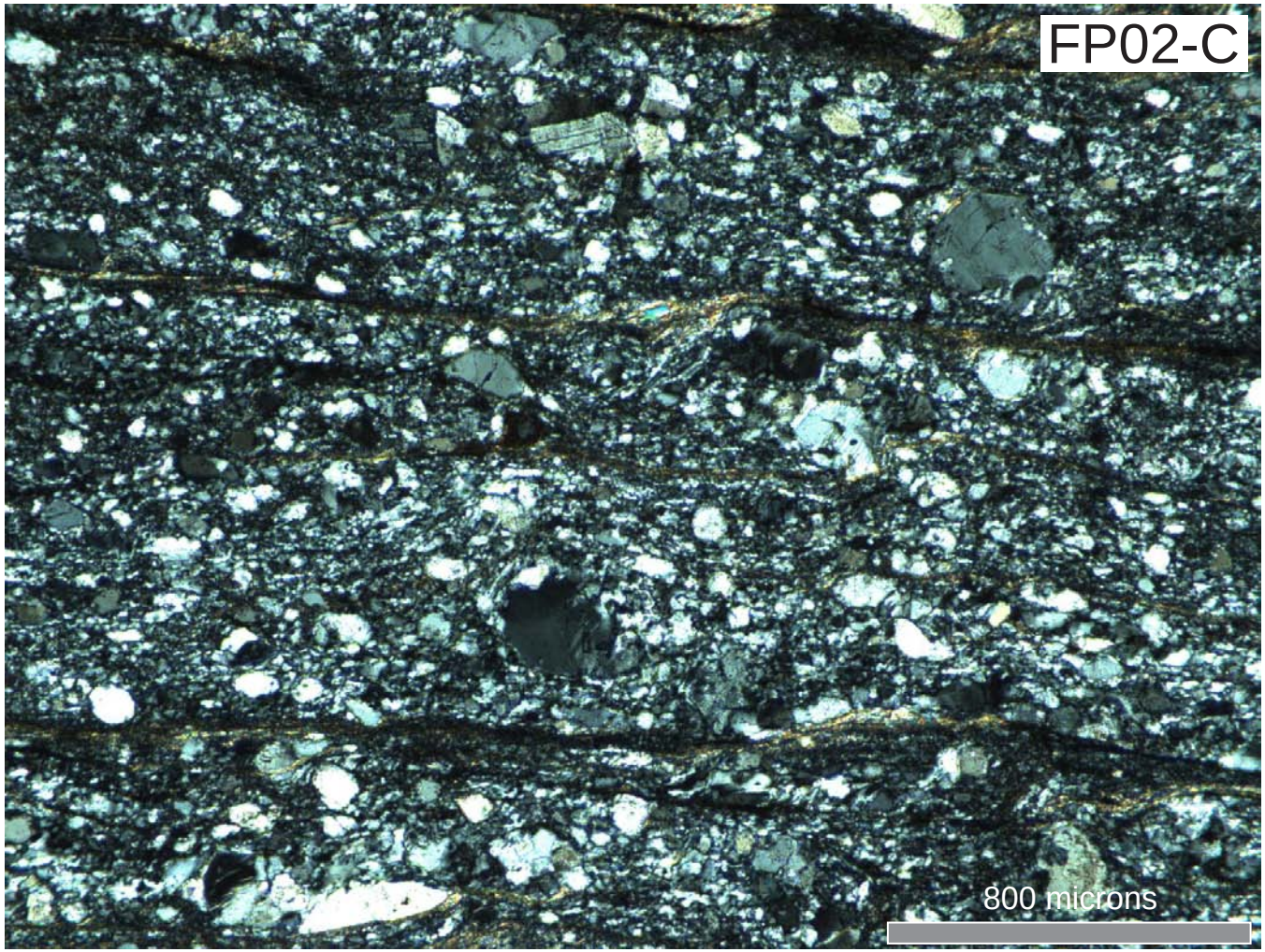

Figure 15.

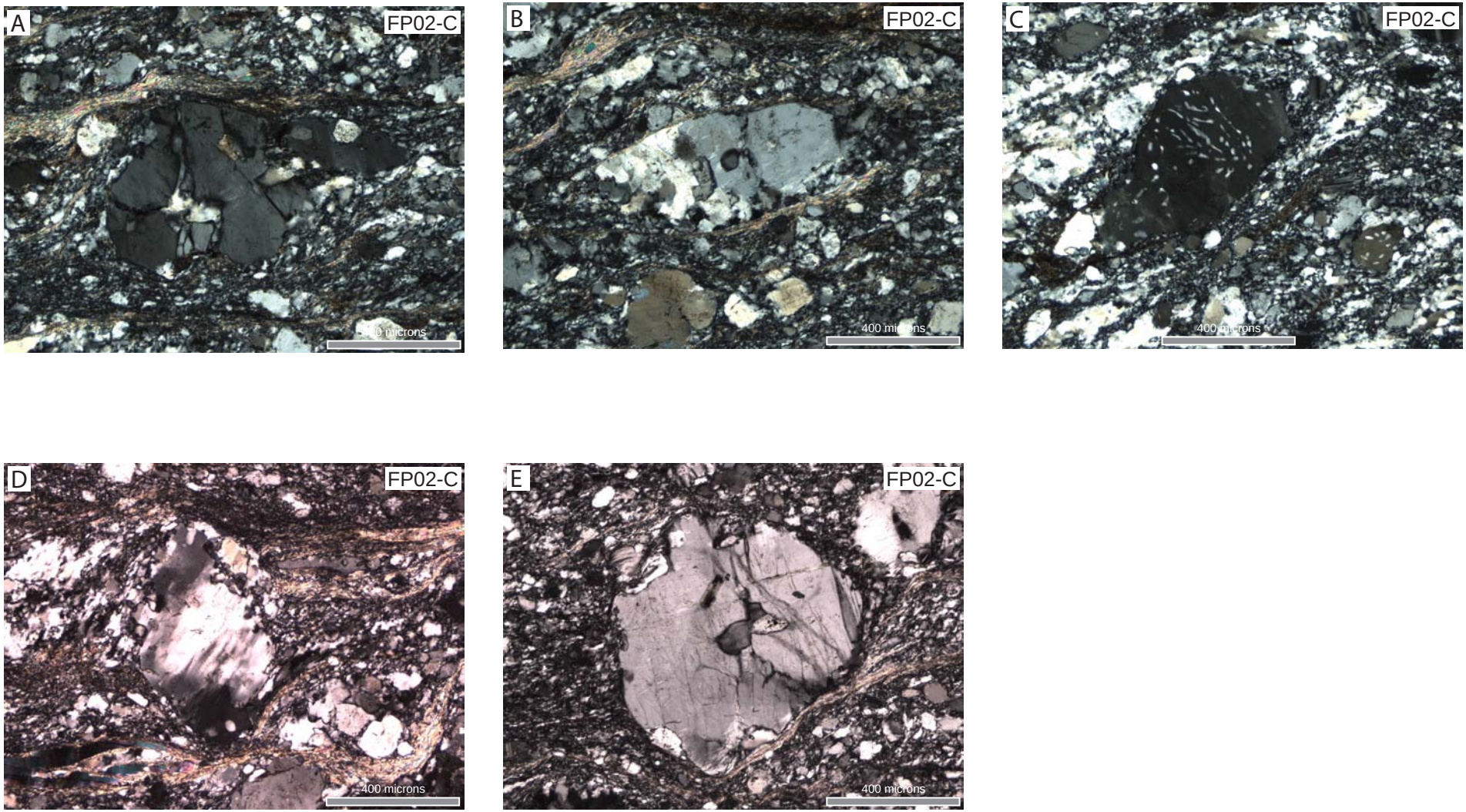
A
FP02-C
400 microns
B
FP02-C
400 microns
C
FP02-C
400 microns
D
FP02-C
400 microns
E
FP02-C
400 microns

Figure 16.

Figure 17.

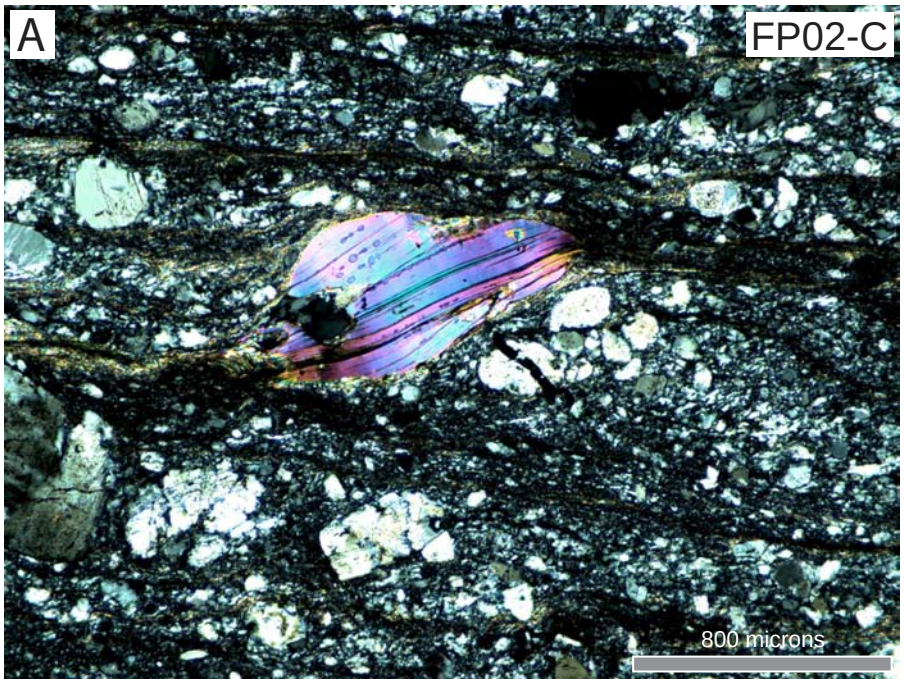

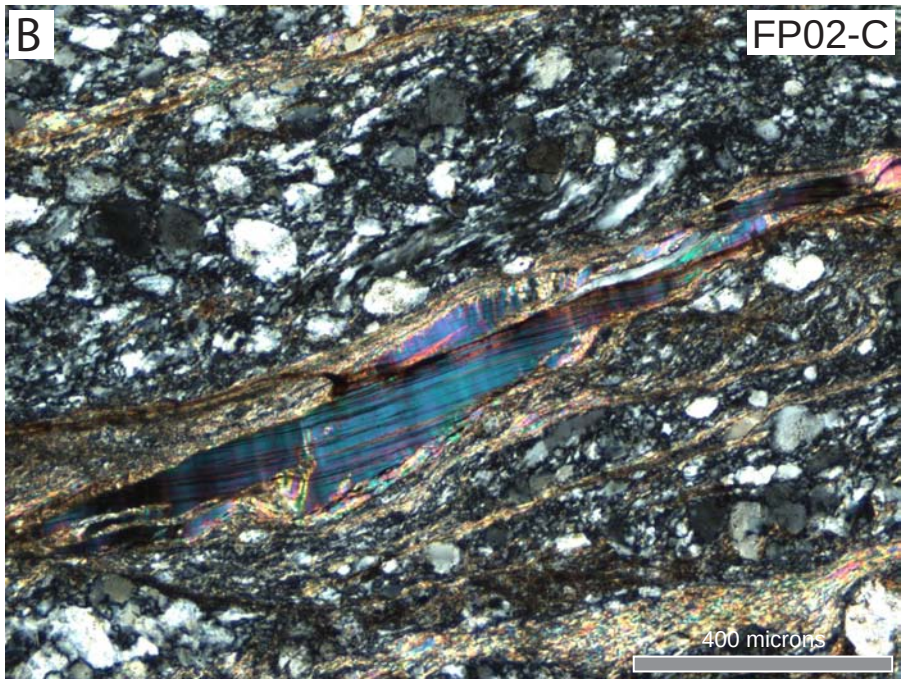

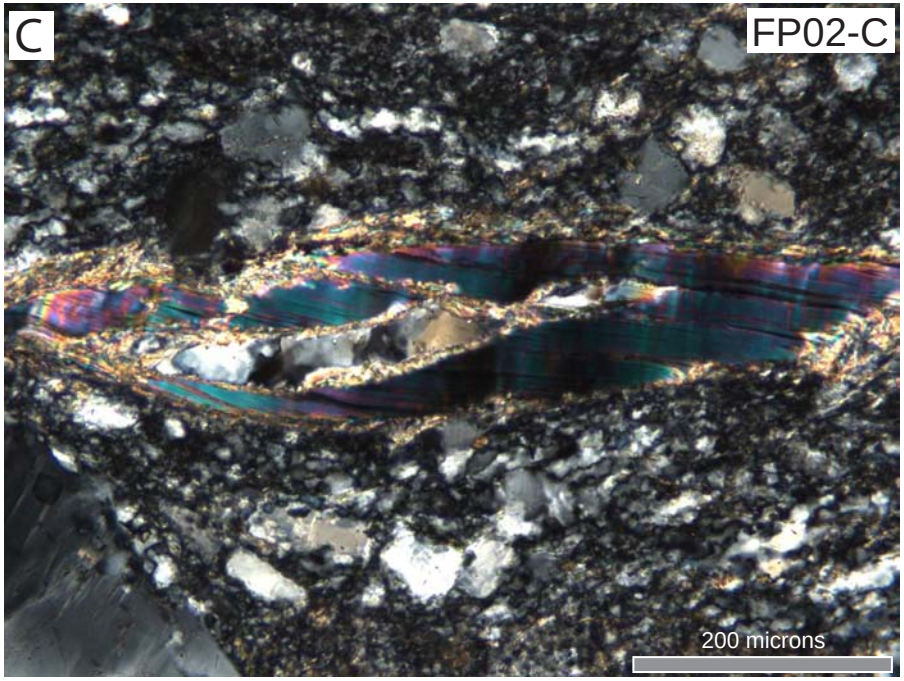

Figure 18.

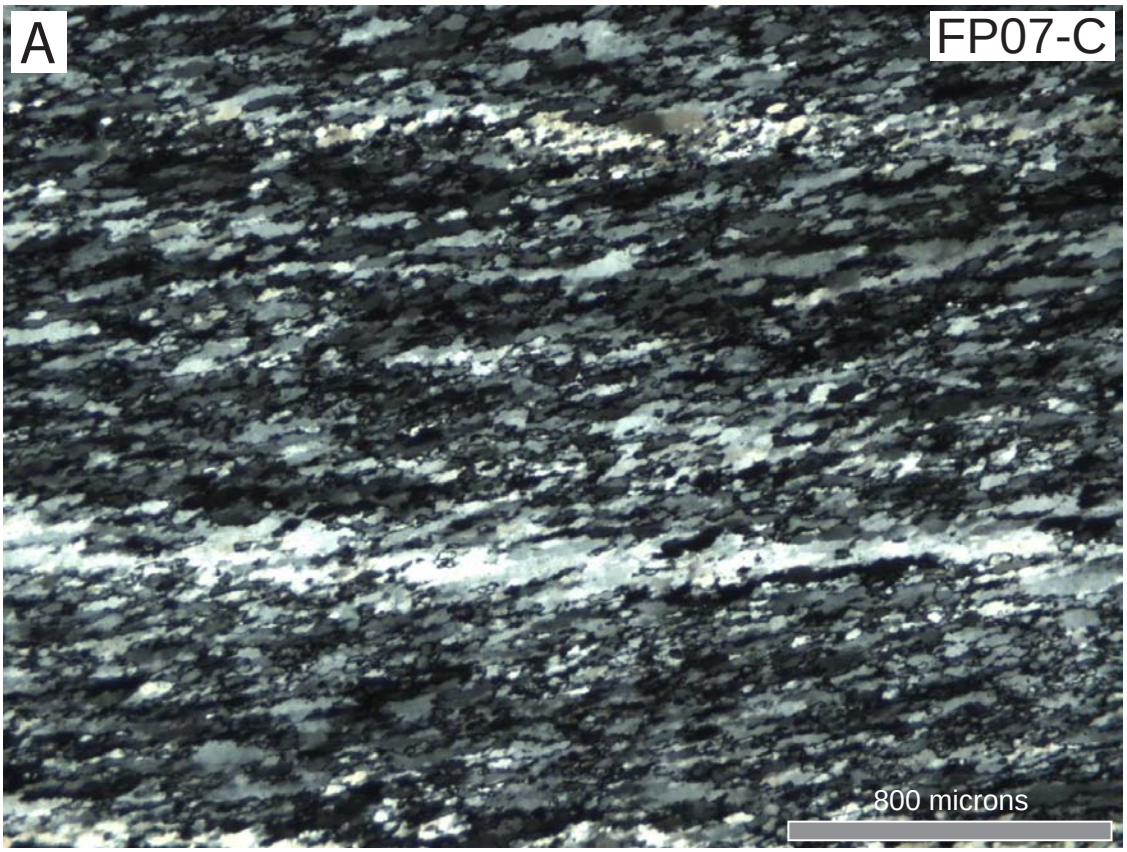

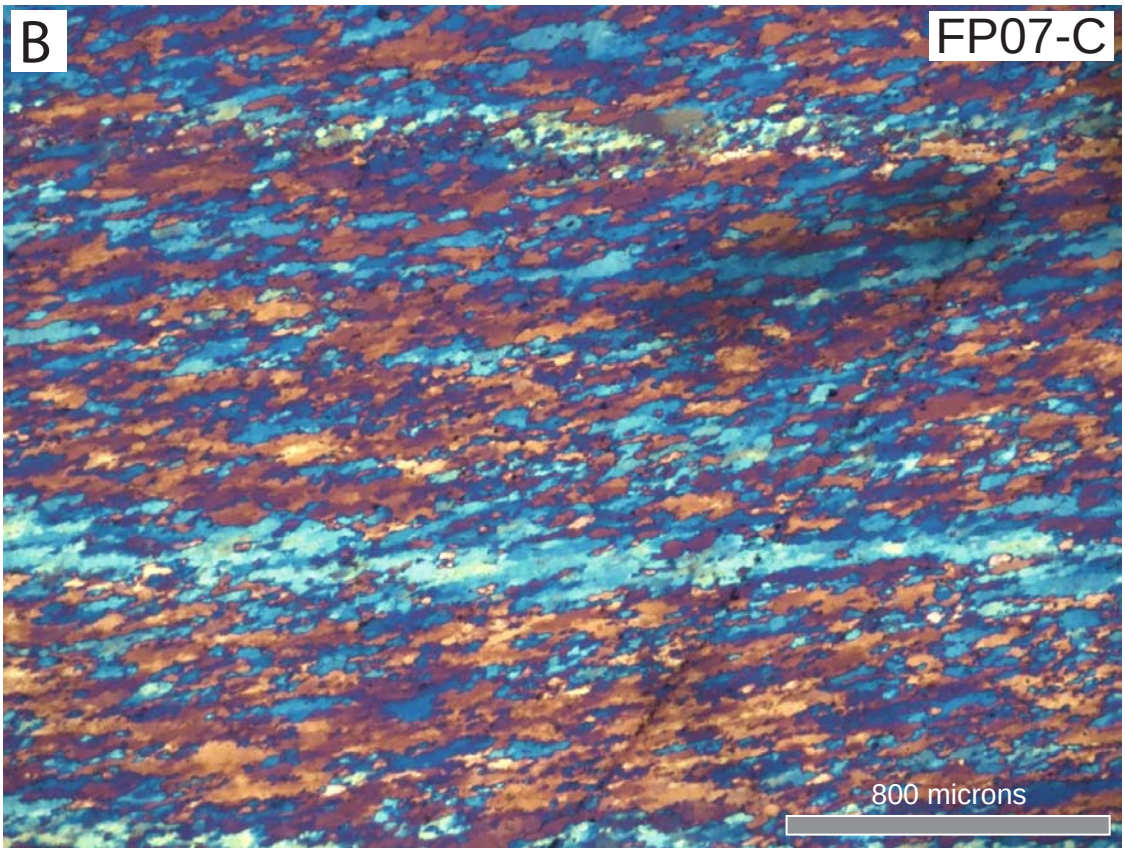

Figure 19.

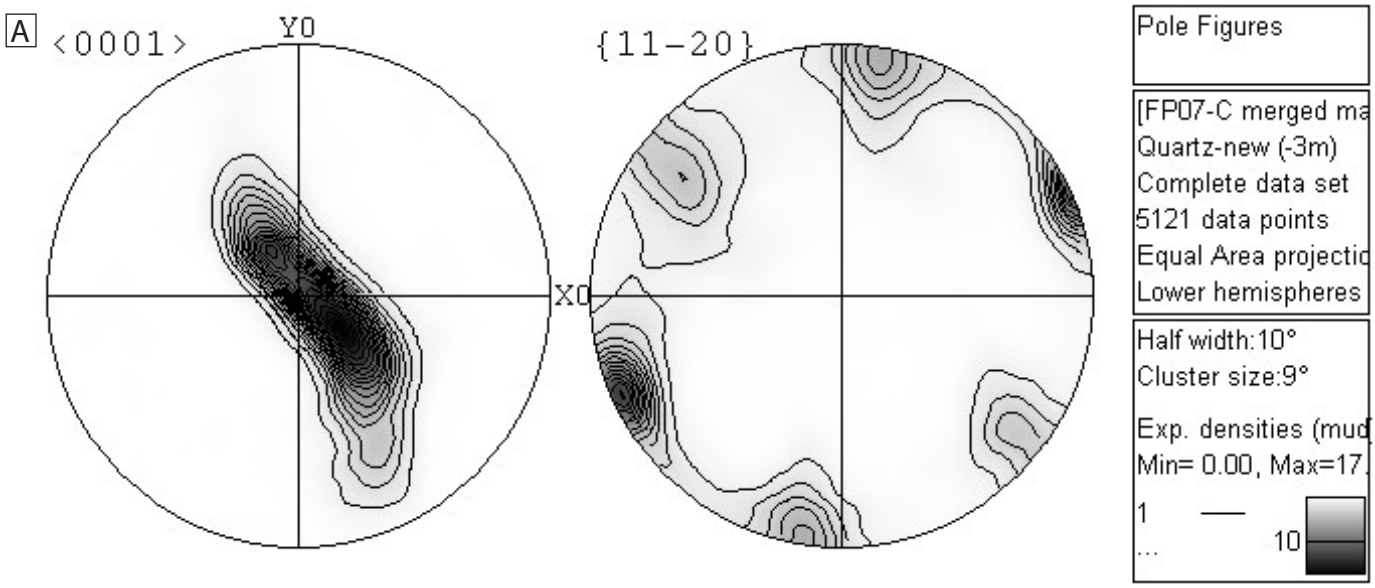
A
<0001>
Y0
X0
{11-20}
Pole Figures
[FP07-C merged ma
Quartz-new (-3m)
Complete data set
5121 data points
Equal Area projectio
Lower hemispheres
Half width:10°
Cluster size:9°
Exp. densities (mud
Min= 0.00, Max=17.
1
10

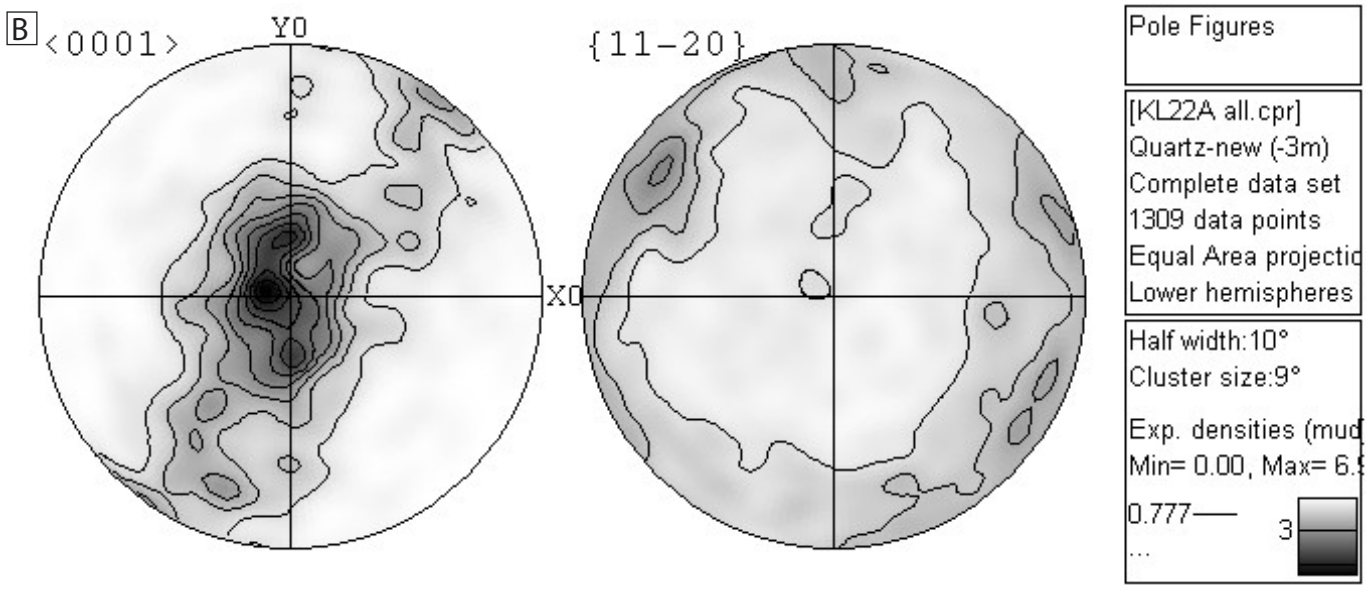
B
<0001>
Y0
X0
{11-20}
Pole Figures
[KL22A all.cpr]
Quartz-new (-3m)
Complete data set
1309 data points
Equal Area projectio
Lower hemispheres
Half width:10°
Cluster size:9°
Exp. densities (mud
Min= 0.00, Max= 6.
0.777
3

Figure 20.